Developments in the Built Environment 25 (2026) 100874

Contents lists available at ScienceDirect

Developments in the Built Environment

journal homepage: www.sciencedirect.com/journal/developments-in-the-built-environment

Low-carbon ternary binder bio-composites via accelerated carbonation for circular construction

Hossein Rahmani [a,**], Hamed Rahimpour [b], Mohammad Reza Hanafi [c], Augonis Algirdas [a,***], Sahar Zinatloo-Ajabshir [d,*]

[a] Faculty of Civil Engineering and Architecture, Kaunas University of Technology, Kaunas, Lithuania
[b] Department of Civil and Construction Engineering, Faculty of Engineering and Science, Curtin University Malaysia, CDT 250, Miri, Sarawak, 98009, Malaysia
[c] Department of Civil & Environmental Engineering, Amirkabir University of Technology, Tehran, Iran
[d] Department of Chemical Engineering, University of Bonab, Bonab, Iran

ARTICLE INFO

Keywords:
Life cycle assessment
Carbon sequestration
Industrial by-products
Pozzolanic reactivity
Microstructural analysis

ABSTRACT

This study demonstrates the significance of coupling biomass valorization with accelerated carbonation curing (ACC) as an integrated strategy for low-carbon construction materials. A bio-based ternary binder incorporating wood sawdust with shale ash, steel slag, and a reduced proportion of ordinary Portland cement (OPC) was developed to simultaneously enhance mechanical performance and enable CO_2 sequestration. The optimized formulation (25% shale ash, 15% OPC, 10% slag, and 50% sawdust) achieved a compressive strength of 7.2 MPa and an elastic modulus of 6 GPa, exceeding the performance of comparable wood-cement composites while using substantially less clinker. Microstructural analyses (SEM, XRD, FTIR, and XPS) confirmed portlandite depletion and the formation of calcite and low-Ca/Si C-(A)-S-H phases under ACC, resulting in matrix densification. Life cycle assessment (EN 15804 +A2) indicated a 65% reduction in greenhouse gas emissions relative to OPC-based systems, highlighting the combined structural and environmental benefits of the proposed approach.

1. Introduction

In recent decades, the built environment has become increasingly recognized as a critical determinant of environmental sustainability and climate resilience. As global urbanization accelerates and infrastructure demands rise, the ecological footprint of construction practices has drawn widespread scientific and policy attention (Wu et al., 2025a). The relentless pursuit of sustainable development within the construction industry has become a paramount global concern, as the inherent environmental impact of conventional building materials, particularly concrete, necessitates a fundamental shift towards eco-conscious alternatives (Ibrahim et al., 2023).

Fundamentally reliant on the use of resource-intensive materials, the construction sector contributes significantly to global greenhouse gas emissions, particularly through the widespread use of concrete. Ordinary Portland cement (OPC), the key ingredient in concrete production, is among the primary anthropogenic sources of CO_2 emissions (Miller and Moore, 2020), positioning the industry as one of the most polluting sectors worldwide. The dramatic rebound in CO_2 emissions (Peters et al., 2012; Wang et al., 2021; Lu et al., 2025), coupled with the rapid growth in concrete demand globally, further underscores the urgency of mitigating its detrimental effects. With cement production accounting for a substantial portion of global CO_2 emissions (Bildirici and Ersin, 2024; Pu et al., 2021), and projections indicating continued growth, especially in developing countries (Ige et al., 2024; Yang et al., 2013), the development of low-carbon alternatives is of utmost importance.

Recent studies have clearly documented the detrimental environmental and health impacts associated with cement production, including air pollution, inefficient resource utilization (Tu et al.), and the risks posed by cement dust exposure (Adeyanju and Okeke, 2019). This trajectory not only threatens environmental sustainability but also imposes a significant economic burden on societies by escalating public health costs. Therefore, reducing the carbon footprint and adopting alternative technologies and materials represent vital pathways toward

* Corresponding author.
** Corresponding author.
*** Corresponding author.
E-mail addresses: hossein.rahmani@ktu.edu (H. Rahmani), algirdas.augonis@ktu.lt (A. Algirdas), s.zinatloo@ubonab.ac.ir, s.zinatloo@gmail.com (S. Zinatloo-Ajabshir).

https://doi.org/10.1016/j.dibe.2026.100874
Received 24 September 2025; Received in revised form 27 January 2026; Accepted 2 February 2026
Available online 10 February 2026

achieving sustainable development goals. In response, researchers are increasingly exploring novel materials and processing techniques (Bontempi et al; Jafari et al., 2025; Mohammadifar et al., 2024) that can significantly lower the environmental burden associated with construction.

In this context, rethinking the building materials supply chain and developing innovative models based on locally available and renewable resources have emerged as key strategies. Utilizing bio-based materials not only addresses ecological challenges but also offers competitive economic advantages at both local and national levels (Le et al., 2023/10). This approach fosters stronger linkages between academic research and industrial needs, creating opportunities for value creation and enhancing community resilience against future uncertainties.

A growing body of research has focused on renewable resources and bio-waste as low-impact alternatives (Hansted et al., 2022; Zhang et al., 2025). Among these, wood which is an accessible bio-based material has shown potential to reduce dependence on conventional materials like cement (Ozcelikci et al., 2024), while facilitating the efficient management of industrial and agricultural waste streams (Czarnecka-Komorowska et al., 2024). This is especially relevant within the framework of recycling-oriented design and the circular economy, where bio-based materials can be engineered for reintegration into the production cycle at the end of their service life. Applications of sawdust, wood ash, and wood biochar in concrete and composites have not only demonstrated promising environmental benefits but also led to significant improvements in selected physical and mechanical properties (Zhang et al., 2024). Specifically, wood-derived biochar, due to its porous structure and chemical stability, can function not only as a filler but also as an active agent for enhancing water absorption control, thermal resistance, and even noise reduction in advanced concrete systems. However, untreated wood contains organic extractives that can significantly retard cement hydration, leading to setting delays and strength loss (Liu et al., 2022; Dias et al., 2022). To address this, methods such as pre-treating the biomass or partially replacing OPC with pozzolanic additives have been employed to improve compatibility and mitigate strength reduction (Dias et al., 2022; Liang et al., 2025).

In parallel, emerging research is exploring the performance of innovative binders such as bio-based binders (Hanafi et al., 2024; Rahmani et al., 2025) and their potential in improving soil mechanical properties and stabilizing subsurface structures (Mollaei et al., 2023). Also, in the field of green construction materials, numerous studies have validated the feasibility of geopolymer materials (Rahimpour and Esmaeili, 2025; Ghiasi et al., 2025; Rahimpour et al., 2024; Fahmi et al., 2023a) and natural binders as partial or complete replacements for cement (Fahmi et al., 2023b; Bualuang et al., 2024, 2025). Beyond their environmental benefits, these binders also offer advantages in terms of human safety, as they are free from hazardous alkalis or heavy metals. In addition to binder innovation, extensive attention has been given to the strategic incorporation of waste-derived materials, particularly wood-based residues such as sawdust and wood ash, to reduce cement consumption and promote circularity. For instance, the partial replacement of OPC with industrial by-products like coal fly ash, silica fume, or ground granulated blast-furnace slag (GGBS) is a well-established strategy to reduce clinker use and enhance long-term concrete performance (Torres-Ortega et al., 2025). Likewise, different ashes from combustion plants exhibits pozzolanic characteristics due to its reactive silica and alumina content, and its incorporation in cementitious mixtures has been shown to improve compressive strength and durability (Prabhath et al.; Khankhaje et al., 2023). Research has shown that wood sawdust can be effectively incorporated into concrete matrices to lower clinker content while maintaining adequate mechanical performance (Ibrahim et al., 2023). Krejsová et al. (2024) investigated waste wood fly ash in lime-based plasters, emphasizing that proper material combinations are critical for strength optimization. He et al. (2022) demonstrated the feasibility of producing magnesium oxychloride cement boards using recycled wood, highlighting the value of resource recovery. Furthermore, Zhang et al. (2024) and Gigar et al. (2023) further emphasized the potential of wood waste inclusion in recycled concrete and geopolymer composites, respectively, underscoring the versatility and environmental benefits of such bio-based amendments.

In parallel with the growing use of bio-based and pozzolanic additives, accelerated carbonation curing (ACC) has emerged as an effective low-temperature route for improving both mechanical performance and environmental compatibility of cementitious systems (Li and Wu, 2022). In ACC, CO_2 reacts with calcium-rich hydration products such as portlandite and C-S-H to form stable carbonate phases (mainly calcite), thereby densifying the microstructure and enabling permanent CO_2 sequestration (Guleria and Goyal, 2025). The efficiency of this process depends on factors such as CO_2 concentration, relative humidity, temperature, and the hydration maturity prior to exposure, which together govern reaction kinetics and depth of carbonation (Padmalal et al.). Recent investigations, including microwave-assisted carbonation of carbide slag-based materials (Lin et al., 2025) and comprehensive reviews on low-carbon concretes have shown that controlled carbonation not only enhances strength and durability but also significantly reduces the embodied carbon footprint of cementitious composites (Liu et al., 2025a).

Despite extensive studies on bio-based fillers, pozzolanic additives, and carbonation curing, these approaches are still predominantly investigated in isolation. Many conventional cement alternatives reduce clinker content or embodied carbon but often compromise mechanical performance, durability, or curing efficiency, particularly when lignocellulosic materials are incorporated. Likewise, carbonation-based strategies are frequently examined without accounting for the interfacial and chemical constraints introduced by biomass-derived fillers. This fragmentation has limited a holistic understanding of the synergistic interactions between biomass valorization and industrial by-products under controlled carbonation conditions. Consequently, a critical gap remains in the absence of an integrated framework that simultaneously couples (i) bio-based material valorization, (ii) pozzolanic mineral replacement, and (iii) accelerated carbonation curing. Previous studies rarely evaluate mechanical, microstructural, and sustainability aspects concurrently, leaving uncertainty regarding their combined potential for low-carbon applications. Accordingly, this study develops a ternary binder system incorporating OPC, shale ash, steel slag, and pretreated wood sawdust, and systematically links its mechanical performance, microstructural evolution, and environmental and social impacts within a unified low-carbon design framework.

2. Materials and methods

This study presents, for the first time, a systematic strategy to develop bio-composites using chemically modified lignocellulosic waste combined with multi-component mineral binders such as OPC, lime, steel slag, and shale ash. By applying targeted chemical treatments and optimized curing protocols, the resulting eco-friendly construction materials exhibit enhanced mechanical performance, long-term durability, and controlled carbonation. This work establishes a framework for valorizing agricultural residues in sustainable, low-carbon, high-performance building materials.

2.1. Materials

Four distinct additive (admixture) solutions were prepared by dissolving specific powders in deionized water at a solid-to-water ratio of 3%. These included: (a) pure water (H_2O), (b) aluminum sulfate ($Al_2(SO_4)_3$) solution with a concentration of 0.03 $kg.L^{-1}$, (c) calcium chloride ($CaCl_2$) solution at 0.03 $kg.L^{-1}$, and (d) calcium hydroxide ($Ca(OH)_2$) solution at 0.03 $kg.L^{-1}$. These compounds served as low-dosage chemical admixtures intended solely for modifying the sawdust surface and enhancing wood-binder compatibility, rather than acting as

hydration or setting accelerators within the binder matrix. Wood sawdust, sourced from untreated wood waste, was precisely dosed at 0.1 kg L^{-1} of each solution. The sawdust was fully immersed in the respective solutions for 24 h at room temperature (25 °C), allowing sufficient chemical interaction to modify the biomass surface properties. After soaking, the material was drained and air-dried under controlled conditions until it reached approximately 20% moisture content (wet basis). This treatment aimed to enhance the reactivity and adhesion potential of the lignocellulosic particles with mineral binders by altering surface functional groups and improving wettability. Following immersion, the sawdust was separated and prepared for subsequent composite formulation. For sawdust pretreatment, $CaCl_2$ and $Al_2(SO_4)_3$ solutions were applied at very low dosages (<1% by binder mass). Their role was limited to improving biomass compatibility, without contributing significantly to binder hydration or carbonation reactions.

The binder system comprised a multi-component mineral matrix consisting of OPC (CEM II 42.5), hydrated lime, steel slag, and calcined shale ash. This formulation was designed to optimize synergistic hydration and carbonation reactions, facilitating the formation of durable calcium silicate hydrate and carbonate phases, thereby promoting mechanical strength and long-term durability.

Since OPC, lime, and shale ash were sourced directly from the factory, their particle fineness was standardized and verified by supplier specifications. Therefore, detailed particle size distributions for these binders were not required. In contrast, the particle size of wood sawdust and steel slag was experimentally determined and reported in Fig. 1, as these non-standard fractions strongly influence binder interaction and composite performance. As illustrated in Fig. 1, the sawdust exhibited a particle size range primarily between 150 and 1000 μm, with a median size (D_{50}) of approximately 450 μm. This relatively coarse and heterogeneous distribution enhances internal porosity and facilitates mechanical interlocking and moisture absorption control within the composite matrix.

2.2. Preparation of samples

High-purity wood sawdust, locally sourced and free from visible contaminants, was selected as the primary lignocellulosic component. To enhance its surface reactivity and compatibility within the binder matrix, the sawdust was subjected to a controlled pre-treatment sequence involving immersion in activating solutions, as illustrated in Fig. 2. Specifically, four distinct pre-treatment solutions were employed, each combining water with either no additive, aluminum sulfate, calcium chloride, or calcium hydroxide (labeled a-d), to induce physicochemical modification at the particle surface. The sawdust was soaked for 24 h at ambient temperature, followed by draining and air-drying until reaching a stable moisture content of approximately 20%. This condition ensured proper workability and optimized interfacial bonding during mixing and curing.

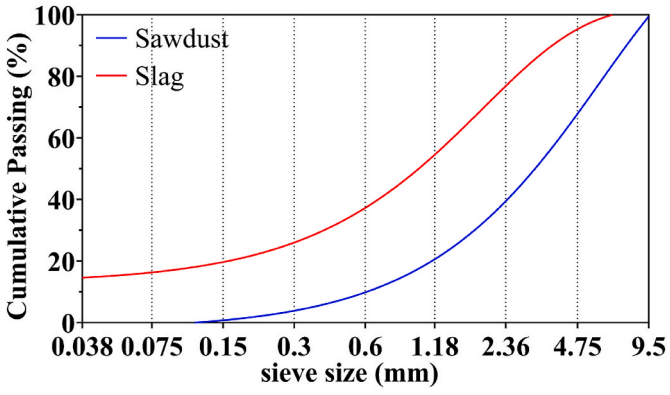

Fig. 1. Particle size distribution curves of wood sawdust and steel slag used in bio-composite production, highlighting the relative coarseness of sawdust particles (150-950 μm) compared to slag (<250 μm).

Prior to pre-treatment, the bulk density of the wood sawdust was determined using the standard relation ρ = M/V, where ρ denotes the bulk density (kg·m^{-3}), M is the mass of the sawdust, and V is its corresponding volume. Measurements indicated that the bulk density of the dry sawdust was approximately 178.5 kg m^{-3}, whereas the wet sawdust exhibited a value of about 340.3 kg m^{-3}. These data provided a reference for moisture absorption capacity and material consistency across all subsequent formulations.

The conditioned sawdust was then mechanically blended with the binder system using a precision-controlled mortar mixer to produce a homogeneous mixture. This ensured uniform dispersion of the organic filler and maximized the effectiveness of matrix–filler interactions during setting and curing. In all formulations, 50 wt% of the total composite consisted of pretreated wood sawdust, which served as the primary bio-based component. The remaining 50 wt% comprised the ternary binder system, with the proportions expressed relative to the total binder mass. Table 1 summarizes the mix design of the binder system together with the type of sawdust pre-treatment and the curing conditions applied in each series.

Fig. 2 provides a schematic representation of the overall fabrication workflow, reinforcing the sequential stages of the process: solution preparation, sawdust treatment, and raw material integration. In alignment with the experimental design, treated sawdust was mixed with complementary binders and mineral additives in a mixing bowl during the integration phase, yielding a cohesive composite paste.

The composite formulation process began with dry blending of the modified sawdust and binder powders for 2 min to ensure initial uniformity. Additive solutions were then incrementally introduced until achieving a water-to-binder ratio (W/B) of 0.5, followed by continuous mixing for five additional minutes to attain a consistent paste. The fresh mix was cast into cubic (10 cm^3), and cylindrical (10 × 10 cm) molds, manually compacted to minimize entrapped air, and sealed to prevent premature moisture loss.

Initial curing was conducted under controlled ambient conditions (25 °C, >95% relative humidity) for 24 h prior to demolding. Thereafter, two distinct curing protocols were employed: a conventional humid curing regime (20 °C, >95% RH for 28 days) to facilitate hydration-driven microstructural evolution, and an accelerated carbonation route conducted in a regulated CO_2 chamber (10-15% CO_2, 65 ± 5% RH, 25 ± 2 °C), aimed at promoting rapid formation of carbonate phases. During accelerated carbonation curing, the chamber was hermetically sealed, and the overall mass variation of specimens was monitored using a precision balance (±0.01 g) to ensure airtightness and to indirectly estimate CO_2 uptake through mass gain tracking. This dual-curing strategy allowed a systematic comparison of hydration-versus carbonation-dominated reaction pathways, providing insight into performance differentiation under varying curing environments.

2.3. Characterization

2.3.1. Mechanical tests

Compressive strength was measured according to ASTM C39 (ASTM C39, 2023) and ASTM C109 (ASTM C109/C109M – 20, 2020), while the elastic modulus was determined using ASTM C469 (ASTM C469-02, 2017). These tests were conducted to quantify the load-bearing capacity and stiffness of the bio-composites, enabling assessment of their structural reliability as cementitious alternatives. Mechanical data also serve as a benchmark to correlate microstructural transformations with macroscopic performance.

2.3.2. Microstructural analysis

Scanning electron microscopy (SEM, JEOL JSM-7800F) was employed to examine interfacial bonding, pore morphology, and fracture characteristics. Surfaces were gold-coated and observed under 5 kV

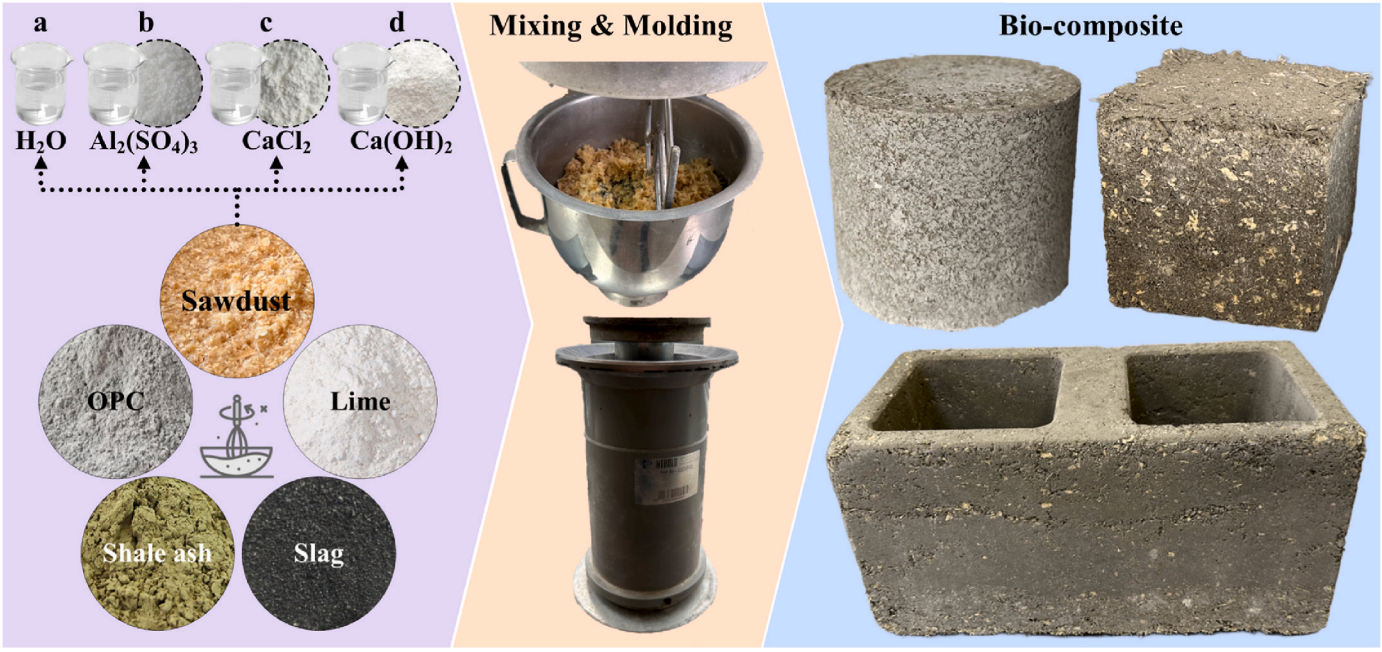

Fig. 2. Schematic overview of the bio-composite fabrication process, including sawdust pre-treatment, binder preparation, mixing, and molding procedures.

Table 1
Mix design (ration) of bio-composites with different binder formulations.

Row	Binders (wt.%)				Wet Sawdust	Pre-treatment	W/B[a]	Curing (day)	
	OPC	Lime	Shale ash	Slag				Ambient	Carbonation
1	100	-	-	-	100	H_2O	0.5	28	-
2	100	-	-	-	100	$Al_2(SO_4)_3$	0.5	28	-
3	100	-	-	-	100	$CaCl_2$	0.5	28	-
4	100	-	-	-	100	$Ca(OH)_2$	0.5	28	-
5	-	100	-	-	100	H_2O	0.5	28	-
6	-	100	-	-	100	$Al_2(SO_4)_3$	0.5	28	-
7	-	100	-	-	100	$CaCl_2$	0.5	28	-
8	-	100	-	-	100	$Ca(OH)_2$	0.5	28	-
10	90	-	10	-	100	H_2O	0.5	28	-
11	80	-	20	-	100	H_2O	0.5	28	-
12	70	-	30	-	100	H_2O	0.5	28	-
13	60	-	40	-	100	H_2O	0.5	28	-
14	50	-	50	-	100	H_2O	0.5	28	-
15	40	-	60	-	100	H_2O	0.5	28	-
16	30	-	70	-	100	H_2O	0.5	28	-
17	20	-	80	-	100	H_2O	0.5	28	-
18	10	-	90	-	100	H_2O	0.5	28	-
19	0	-	100	-	100	H_2O	0.5	28	-
20	45	-	50	5	100	H_2O	0.5	28	-
21	40	-	50	10	100	H_2O	0.5	28	-
22	35	-	50	15	100	H_2O	0.5	28	-
23	30	-	50	20	100	H_2O	0.5	28	-
24	25	-	50	25	100	H_2O	0.5	28	-
25	20	-	50	30	100	H_2O	0.5	28	-
26	15	-	50	35	100	H_2O	0.5	28	-
27	10	-	50	40	100	H_2O	0.5	28	-
28	5	-	50	45	100	H_2O	0.5	28	-
29	30	-	50	20	100	H_2O	0.35	28	-
30	30	-	50	20	100	H_2O	0.4	28	-
31	30	-	50	20	100	H_2O	0.45	28	-
32	30	-	50	20	100	H_2O	0.55	28	-
33	30	-	50	20	100	H_2O	0.5	28	-
34	30	-	50	20	100	H_2O	0.5	27	1
35	30	-	50	20	100	H_2O	0.5	26	2

[a] Water-to-binder ratio.

accelerating voltage and 10 mA beam current across multiple magnifications. This analysis aimed to elucidate the role of biomass–binder interactions, microcrack propagation, and densification mechanisms in governing mechanical performance.

2.3.3. Phase composition

X-ray diffraction (XRD, PANalytical X'Pert PRO, Cu Kα) was performed over a 10-70° 2θ range to identify crystalline phases, while X-ray fluorescence (XRF, PANalytical Axios) quantified major oxides. These tests were designed to reveal hydration, pozzolanic, and carbonation products, as well as chemical shifts induced by shale ash and slag incorporation. Establishing links between oxide composition, phase assemblage, and strength development was essential for validating binder optimization.

Additionally, Fourier Transform Infrared (FTIR, Bruker Tensor 27) spectroscopy was used to analyze the bonding environments and functional groups within the binder matrix (400-4000 cm^{-1}). The spectra complemented XRD and XRF results by identifying portlandite consumption, carbonate formation, and Si-O-T band shifts, confirming the development of low-Ca/Si C-(A)-S-H gels and extensive carbonation.

2.3.4. Surface chemical states

X-ray photoelectron spectroscopy (XPS, JEOL JPS-9030, Al Kα, $\sim 10^{-9}$ mbar) provided insights into oxidation states, bonding environments, and carbonation-induced surface modifications. Survey and high-resolution spectra were analyzed using CasaXPS. The objective was to capture nanoscale chemical environments at the wood–matrix interface and verify mechanisms of Ca/Si/Al rebalancing, which underpin enhanced durability and low-carbon performance.

2.3.5. Sustainability and social assessments

Life cycle assessment (LCA) was conducted following ISO 14040/44 () and EN 15804+A2 (EN 15804+A2, 2019) with a cradle-to-gate system boundary. Data sources included Ecoinvent v3.8, industrial records for shale ash/slag, and laboratory measurements. Impacts across 12 categories were quantified using ReCiPe 2016 and EN 15804+A2, and monetized through eco-cost analysis. The LCA aimed to evaluate the environmental footprint of the bio-composites versus OPC-based systems, highlighting the benefits of clinker reduction and CO_2 uptake via accelerated carbonation curing (ACC). The functional unit (FU) was defined as 1 m^3 of bio-composite for non-load-bearing applications under standard curing. The reference service life (RSL) was assumed to be 25 years, following EN 15804 +A2 guidelines. Both systems were compared under functional equivalence, ensuring similar mechanical performance (≥7 MPa at 28 days) and service function. This approach guarantees a transparent, performance-based comparison of key impact indicators such as global warming potential (GWP), ADP, and PED. Furthermore, end-of-life (Modules C1-C4) was modeled as landfill with partial energy recovery, while circularity refers to waste valorization in production (A1-A3); no Module D credits were included to avoid double counting in accordance with EN 15804+A2.

Inventory data for shale ash and steel slag were obtained from verified industrial process information and cross-checked with representative datasets from Ecoinvent v3.8 to ensure consistency and completeness. Differences in energy intensity between the sources were below 5%, confirming their compatibility for LCA use. Transportation was modeled as regional road freight with an average 50 km distance using EURO 6 trucks. Electricity consumption for raw material drying and accelerated carbonation curing (ACC) was based on metered laboratory values (0.6-0.8 kWh per kg of binder) and included directly in the life cycle inventory. CO_2 uptake during ACC was modeled as a negative emission flow in accordance with EN 15804+A2 (Modules A1-A3). The absorbed CO_2 was quantified from specimen mass gain, corrected by subtracting the negligible mass change of control samples cured without CO_2 exposure. CO_2 uptake during ACC was modeled as a negative emission flow under Module A3, following EN 15804+A2 and EN 16757. The uptake reflects the verified sequestration occurring during the controlled ACC process, quantified from specimen mass gain and corrected against non-carbonated controls. No additional CO_2 uptake was assigned to the use or end-of-life stages, thereby preventing double counting between modules and ensuring transparency in the carbon balance.

The social life cycle assessment (S-LCA), based on the UNEP/SETAC framework, addressed worker health and safety, job creation, wage equity, and community reinvestment, using labor statistics from cement and biomass recycling sectors. The aim was to demonstrate the socio-economic value of biomass and industrial waste integration, thereby positioning the material not only as technically viable but also as socially responsible.

3. Results and discussion

The tests conducted in this study are organized into four complementary categories-physical, chemical, microstructural, and sustainability analyses, providing a comprehensive evaluation of the bio-composites from both performance and environmental perspectives. Physically, compressive strength, density, and elastic modulus were measured simultaneously to understand load-bearing behavior and structural integrity. Chemically, advanced techniques such as XRD, XRF, XPS, and elemental analysis were used to investigate phase composition, elemental distributions, and surface chemistry, elucidating key material transformations. SEM analysis further characterized microstructural features such as matrix densification, porosity, crack propagation, and interfacial bonding with wood sawdust. Finally, sustainability considerations, including clinker reduction, carbonation curing, and the use of industrial by-products were assessed to evaluate the environmental benefits of the optimized formulations. This integrated approach enables robust correlations between mechanical performance, chemical and microstructural characteristics, and environmental impact, offering insight into how binder selection and curing conditions govern the behavior and sustainability of wood sawdust-based bio-composites.

3.1. Effect of pre-treatment on binders

This study aimed to evaluate the influence of binder type and chemical pre-treatment on the mechanical and physical performance of wood sawdust-based biocomposites. Two mix designs comprising 100% OPC and 100% Lime with identical weight ratios were examined under four different pre-treatment conditions: pure water, aluminum sulfate, calcium chloride, and calcium hydroxide. The focus of this research was to determine the precise effects of these variables on compressive strength, density, and modulus of elasticity, enabling a comparative analysis to elucidate functional mechanisms and potential improvements in the mechanical behavior of wood-mineral biocomposites. This approach facilitates the identification of optimal formulations for the production of lightweight and durable building materials, particularly with the objective of incorporating bio-based resources and reducing environmental impacts.

Analysis of the results reveals that the mechanical and physical performance of biocomposites made with 100% OPC and 100% Lime is strongly affected by the type of chemical pre-treatment applied to the sawdust. As shown in Fig. 3, in the control condition (pre-treatment with pure water), the OPC-based biocomposite exhibited a compressive strength of 2.80 MPa, density of 1.384 g cm^{-3}, and modulus of elasticity of 3.70 GPa, which were significantly higher than the corresponding Lime-based specimens (0.80 MPa, 0.934 g cm^{-3}, and 1.10 GPa, respectively). This confirms that OPC-based binders, due to more extensive hydration and the formation of cementitious products, produce a denser and more cohesive structure than Lime-based systems (Adem et al., 2025; Naseri et al., 2025; Asheghi Mehmandari et al., 2024a). Also, stress state also influences compressive strength and failure patterns (Zhou et al., 2025). While previous studies have established that processing conditions can influence mechanical properties in wood-based bio-composites (Chen et al., 2024), the present work uniquely demonstrates how targeted chemical pre-treatment combined with hybrid mineral binders governs the development of elastic modulus in high wood-content cementitious systems.

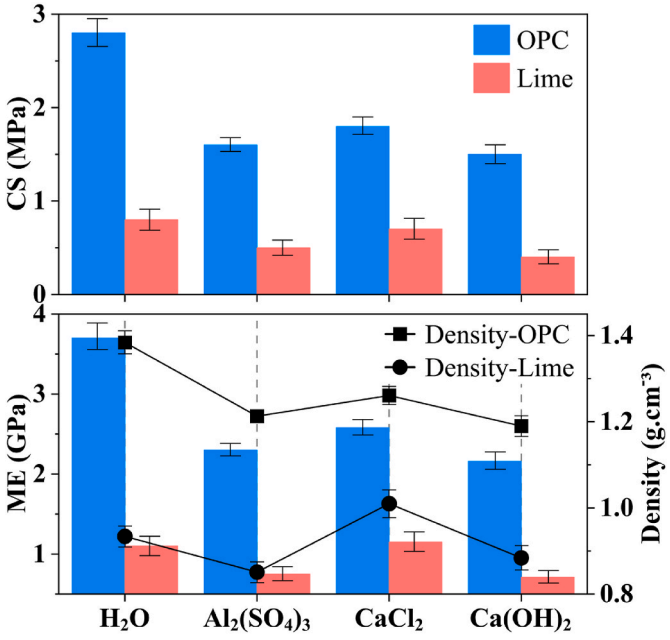

Fig. 3. Mechanical and physical properties (compressive strength, elastic modulus, and density) of 100% OPC and 100% Lime bio-composites prepared with different sawdust pre-treatment types (Water, CaCl2, $Al_2(SO_4)_3$, $Ca(OH)_2$).

The use of chemical pre-treatments had a significant influence on mechanical properties. For example, pre-treatment with aluminum sulfate resulted in a reduction in compressive strength for both systems: compressive strength decreased to 1.60 MPa for OPC (approximately 43% reduction compared to the control) and to 0.50 MPa for Lime (approximately 38% reduction). A decline in both density and modulus of elasticity was also observed, likely due to the formation of Al^{3+} complexes with lignin and cellulose in the sawdust, which inhibits hydration reactions and interfacial bonding between the wood particles and the mineral matrix.

Careful examination of Fig. 3 reveals that specimens pre-treated with calcium chloride showed a relative improvement in mechanical performance, particularly for Lime-based composites. Compressive strength for OPC increased to 1.80 MPa, approximately 12.5% higher than the aluminum sulfate case, and for Lime to 0.70 MPa (a 40% increase). This may be attributed to the role of calcium chloride as an accelerator for hydration reactions, which, even in the presence of lignocellulosic fillers, enhances the rate and extent of cementitious product formation (Steger et al., 2021). The increase in density to 1.261 g cm^{-3} for OPC and 1.010 g cm^{-3} for Lime further supports the presence of a denser microstructure in these conditions. Additionally, the enhancement in modulus of elasticity to 2.58 GPa for OPC and 1.15 GPa for Lime reflects an overall increase in composite stiffness. Comparable improvements in stiffness have been reported in wood-plastic and bio-polymer composite systems, where increased wood filler content, particularly sawdust was shown to enhance stiffness and load resistance through better matrix-particle interlocking.

In the case of calcium hydroxide pre-treatment, a more pronounced decline in mechanical properties was observed: compressive strength dropped to 1.5 MPa for OPC (approximately 46% reduction compared to control) and 0.4 MPa for Lime (50% reduction). This could be due to the formation of excessive lime precipitates and elevated local pH, which diminishes compatibility between the wood filler and the mineral matrix (Kang et al., 2025). The lowest densities were also recorded in these specimens (1.19 g cm^{-3} for OPC and 0.884 g cm^{-3} for Lime), indicating a more open and porous structure.

Across all cases, OPC-based systems consistently outperformed Lime-based systems by a factor of approximately 2 to 3 on average. This can be attributed to the fundamental differences in the hydration behavior of these binders; while OPC generates a dense network of cementitious products, Lime primarily engages in slower and more limited reactions with sawdust, resulting in weaker and more porous structures. These findings are consistent with prior research on natural polymer composites, where lignocellulosic reinforcements such as sawdust and coniferous bark were shown to enhance elastic modulus and flexural performance (Jinanukul et al., 2024). At the same time, the current results underscore that the inherent inhibitory effects of lignocellulosic compounds on cement and lime hydration can be effectively mitigated through appropriate chemical pre-treatment, particularly with calcium chloride thereby enabling the development of structurally robust, wood-based biocomposites. The improved interfacial bonding observed in $CaCl_2$-and $Al_2(SO_2)_3$-treated sawdust composites can be attributed to partial removal of extractives and surface neutralization, which increased surface energy and enhanced wettability. This facilitated stronger adhesion with the cementitious matrix while simultaneously moderating internal water retention, thereby improving both workability and long-term dimensional stability.

Overall, a review of Fig. 3 suggests that the combined selection of binder type and pre-treatment significantly influences the compressive strength, density, and modulus of elasticity of these biocomposites. While pure water provided the best performance in both systems, calcium chloride emerged as an effective pre-treatment, particularly in combination with OPC. Given that the specimens pretreated with pure water consistently exhibited the highest mechanical strength and densification across both binder systems, this condition was selected as the primary pretreatment approach for all subsequent mix designs and analyses throughout the study.

3.2. *Influence of shale ash and slag replacements*

In this section, the mechanical and physical performance of biocomposites containing wood sawdust was optimized by evaluating the gradual replacement of OPC with two sustainable mineral substitutes, shale ash and slag. The use of such industrial by-products has attracted increasing interest due to their pozzolanic activity and ability to reduce cement clinker content, a factor crucial for mitigating CO_2 emissions. Previous studies have shown that slag, particularly ladle furnace slag and arc gasification slag can yield compressive strengths comparable to or even higher than those of pure cement systems when properly proportioned and treated (Araos Henríquez et al., 2021; Liu et al., 2025b). In the present study, this replacement strategy was not treated in isolation but as part of an integrated experimental matrix, allowing the interaction between binder type, biomass fraction, and curing regime to be captured explicitly. This provides a sound foundation for evaluating the synergistic potential of slag and shale ash as complementary components in low-OPC biocomposite formulations.

Based on the preliminary results, the formulation incorporating OPC with water-pretreated sawdust was identified as the most efficient configuration and was selected as the baseline for specimen preparation used in subsequent experimental stages. Subsequently, interaction effects were examined by varying shale ash content while holding the biomass fraction constant, and then by introducing slag as an additional variable. First, different percentages of Shale ash were examined as partial replacements for OPC to identify the optimal replacement level. Then, using the optimal Shale ash content, part of the remaining OPC was replaced with slag to further improve compressive strength and mechanical performance. The primary objective of this study was to achieve the highest compressive strength and stiffness while maintaining structural density and significantly reducing OPC consumption which is the most carbon-intensive component through the incorporation of industrially available, reactive, and sustainable mineral materials to develop high-performance, sustainable construction bio-composites.

The results of progressively replacing OPC with Shale ash in composites containing wood sawdust revealed a nonlinear trend highly

dependent on replacement percentage. This nonlinear response indicates that the mechanical behavior is governed by interaction between the alkaline environment provided by OPC and the pozzolanic reactivity of shale ash. As evident from Fig. 4, in the initial mixture without Shale ash (100% OPC), compressive strength, elastic modulus, and density were 2.80 MPa, 3.69 GPa, and 1.382 g cm^{-3}, respectively, which served as the reference. Adding 10% Shale ash (reducing OPC to 90%) increased compressive strength to 3.3 MPa and elastic modulus to 4.01 GPa. The improvement continued with 20% and 30% Shale ash replacements, reaching 4 MPa and 4.9 MPa (a 43% and 75% increase compared to the initial mix), while elastic modulus improved to 4.91 GPa at 15% replacement.

The highest performance was achieved at 50% Shale ash replacement (i.e., 50% Shale ash, 50% OPC). As shown in Fig. 4, compressive strength peaked at this point: 6.10 MPa (over a 118% increase relative to the baseline), elastic modulus increased to 5.51 GPa, and density rose slightly to 1.391 g cm^{-3}, indicating a compact structure. This enhancement is likely due to the pozzolanic reactivity of Shale ash in the alkaline environment provided by OPC, demonstrating the combined effect of both binders rather than the action of a single component. These results align with previous studies on the use of pozzolanic materials in cementitious systems (Alaloul et al., 2024; Moodi et al., 2025) and underscore the environmental relevance of partially replacing OPC with industrial by-products like Shale ash. Further increases in Shale ash content beyond 50% resulted in a gradual decline in performance: compressive strength dropped to 4.80 MPa at 60% replacement and declined further to 2.50 MPa and 2.00 MPa at 90% and 10% replacements, respectively.

After identifying 50% Shale ash as the optimal replacement level, the effect of progressively replacing part of the remaining OPC with slag was examined to achieve further mechanical enhancement and environmental benefits. The reference mix for this stage comprised 50% Shale ash, and 50% OPC. Slag was then introduced to replace part of the remaining OPC. Here, the study design explicitly probed the three-way interaction among shale ash, slag, and OPC content. Replacements up to 20% slag (i.e., 50% Shale ash, 30% OPC, 20% slag) led to a continuous improvement in properties; as observed in Fig. 4, compressive strength increased from 6.10 MPa to 6.50, 6.70, 6.90, and ultimately 7.2 MPa at 20% slag (an approximately 18% increase over the reference). Elastic modulus also improved from 5.50 GPa to 6.01 GPa. This trend illustrates that the beneficial effect is not additive but arises from the synergistic interaction of slag with the existing ash-OPC system. The increasing compressive strength and modulus of elasticity observed in this phase of the study are consistent with previous research. Dong et al. (2021) reported that proper treatment and proportioning of steel slag in cementitious systems significantly enhances the long-term performance and durability of concrete, which aligns with the densification trends and strength gains identified in the slag-containing formulations of the present study.

Density exhibited a slight upward trend during this stage: from 1.393 g cm^{-3} at 0% slag to 1.395 g cm^{-3} at 20% slag. This minor increase in density can be attributed to the inherently higher density of slag compared to Shale ash, contributing to a greater specific mass of the composite while maintaining or even improving microstructural compactness. This behavior confirms that the introduction of slag does not induce additional porosity but rather supports structural densification.

At slag replacement levels beyond 20%, a gradual reduction in performance occurred: compressive strength decreased to 6.90 MPa at 25% slag, 6.40 MPa at 30%, and 5.20 MPa at 45% slag, while elastic modulus decreased from 6.01 GPa to 5.08 GPa at 45% slag. This decline further illustrates how interaction effects shift once the balance between OPC, slag, and shale ash is disrupted, limiting hydration reactions. These findings also support conclusions by Tsakiridis et al. (2008), who emphasized that the introduction of steel slag into cement systems not only promotes strength development but also enables a measurable decrease in cement clinker usage which is an aspect of growing environmental significance. Cai et al. (2024) further underlined that the pozzolanic effectiveness of slag is closely tied to its chemical composition, an observation reflected here through the superior performance of

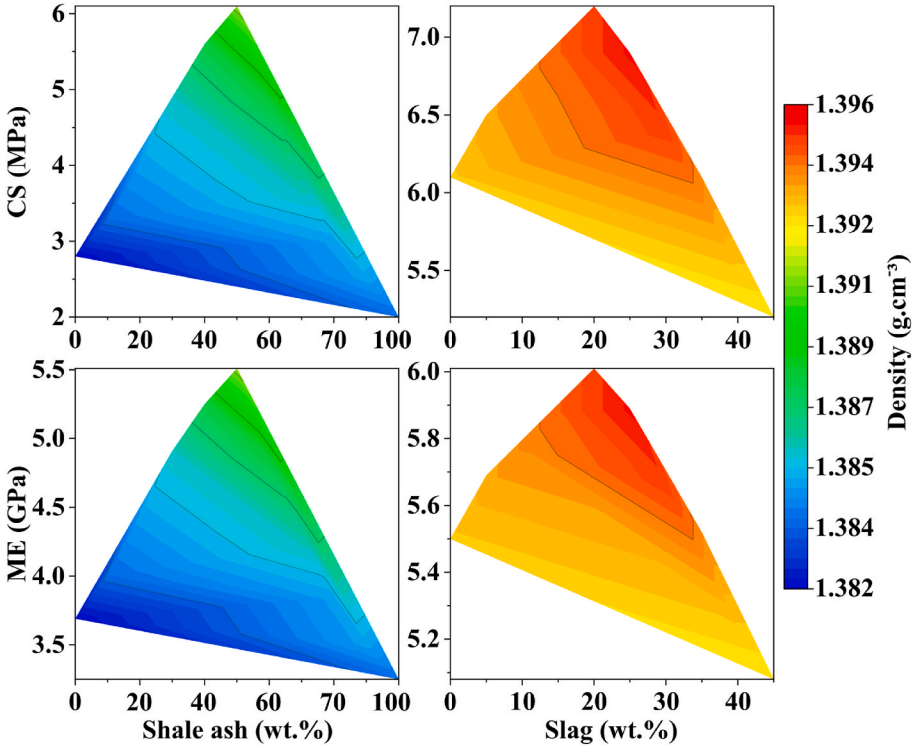

Fig. 4. Variation of compressive strength, elastic modulus, and density of wood sawdust bio-composites as a function of shale ash and slag replacement levels for OPC binder.

mixtures containing both slag and shale ash with balanced oxide content.

Overall, the composition containing 50% Shale ash, 30% OPC, and 20% slag was identified as the optimal mix in terms of mechanical performance and structural density; Fig. 4 clearly indicate that this mix exhibited the highest performance among all tested formulations, achieving a compressive strength of 7.2 MPa (more than 2.5 times the initial mix without Shale ash and slag) and an elastic modulus of 6.01 GPa, while maintaining an appropriate density of approximately 1.395 g cm^{-3}. By framing these results as outcomes of binder–filler–curing interactions, the study demonstrates not only the effect of individual substitutions but also the underlying synergy that governs the mechanical performance of bio-composites. Although the composite exhibits notable compressive strength and stiffness, it is intended for non-load-bearing applications where lightweight structure, environmental performance, and dimensional stability are prioritized over fracture or flexural resistance.

3.3. Role of W/B ratio

Following the optimization of bio-composites composed of 50% Shale ash, 30% OPC, and 20% slag along with wood sawdust identified in the previous stages, the water-to-binder ratio (W/B) was evaluated as a key parameter influencing mechanical and physical properties. Adjusting the W/B ratio can have multiple effects on mix workability, compaction degree, hydration reactions, and ultimately on microstructure and mechanical performance; therefore, identifying the optimal W/B ratio is essential to ensure maximum composite performance. Importantly, this stage of the study was designed not as an isolated parameter test, but to reveal how water availability interacts with the previously optimized binder composition and carbonation curing regime, thereby capturing interaction effects between mix design and curing chemistry. This behavior aligns with prior evidence showing that optimal water-to-binder ratios enhance strength and reduce porosity by improving hydration efficiency and matrix densification (Yilmazoglu et al., 2024; Nguyen et al., 2021).

As evident from Fig. 5, at a W/B ratio of 0.35, compressive strength, elastic modulus, and density were recorded as 6.2 MPa, 5.57 GPa, and 1.393 g cm^{-3}, respectively, slightly below the optimal values obtained in the previous phase. Increasing the W/B ratio to 0.4, 0.45, and ultimately 0.5 led to a continuous improvement in mechanical performance: compressive strength rose from 6.4 MPa at 0.4 to 6.8 MPa at 0.45, reaching a peak of 7.2 MPa at 0.50 (representing a 16% increase relative to 0.35). Correspondingly, elastic modulus increased from 5.66 GPa at 0.4 to 5.84 GPa at 0.45 and 6.01 GPa at 0.5. This progressive improvement highlights the synergy between increased water availability and the pozzolanic activity of shale ash and slag, which together promote more complete hydration–carbonation reactions.

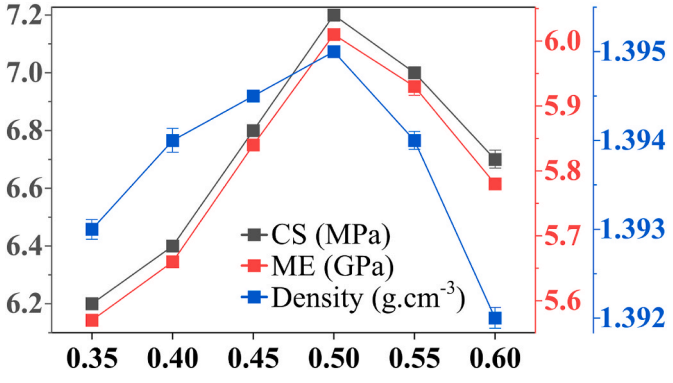

Fig. 5. Effect of water-to-binder ratio (W/B) on compressive strength, elastic modulus, and density of optimized wood sawdust-based bio-composites containing 50% shale ash, 30% OPC, and 20% slag.

This enhancement can be attributed to improved workability, better packing density, and reduced porosity resulting from sufficient water availability. Within this W/B range, additional water likely contributed fully to hydration reactions, leading to a uniform and dense microstructure. According to Fig. 5, density remained nearly constant at approximately 1.394 to 1.395 g cm^{-3} across this range, indicating no excessive porosity and ensuring a compact structure.

Further increases in W/B to 0.55 and 0.6 resulted in a gradual decline in mechanical performance: compressive strength decreased to 7 MPa and 6.7 MPa, while elastic modulus declined to 5.93 GPa and 5.78 GPa, respectively. This reduction is likely due to excessive water leading to increased porosity upon evaporation and weakening of matrix bonds. These results confirm that water addition beyond the optimum disrupts the positive interaction observed earlier, showing that durability and performance are governed by a delicate balance between water content and binder chemistry. This trend is consistent with earlier findings on cementitious and lignocellulosic composites, where controlling the water-to-solid ratio below a critical threshold has been shown to enhance mechanical performance by improving hydration, reducing capillary porosity, and promoting matrix densification (Badalyan et al., 2024).

Overall, Fig. 5 clearly show that a W/B ratio of 0.5 delivered the best mechanical performance, yielding a compressive strength of 7.2 MPa and an elastic modulus of 6.01 GPa, while density remained stable at approximately 1.395 g cm^{-3}, ensuring optimal compaction and minimal porosity. By framing W/B not only as a single variable but as an interactive factor with binder composition and curing conditions, the study demonstrates that maximum performance is achieved when water content, pozzolanic reactivity, and carbonation curing are jointly optimized.

These results confirm the importance of optimizing the water-to-solids ratio alongside the design of an optimal mixture incorporating mineral alternatives to OPC (Shale ash and slag) and sustainable bio-based materials such as wood sawdust. Precise adjustment of W/B not only enables maximum strength and stiffness but also prevents excessive water content and its negative effects on microstructure and durability.

3.4. Effect of curing conditions

Following the optimization of the bio-composites composed of 50% Shale ash, 30% OPC, 20% slag, and a W/B ratio of 0.5 identified in previous stages, this section investigates the effect of different carbonation curing regimes on mechanical properties and density. In this experiment, the control sample was subjected to standard ambient curing with no carbonation, while other samples were exposed to CO_2 curing under three distinct scenarios: (a) immediate carbonation after casting (0-day delay), (b) carbonation after a 1-day delay, and (c) carbonation after a 2-day delay. Each scenario included curing durations of either 1 or 2 days in a CO_2 environment, allowing evaluation of both the carbonation delay and carbonation period. By structuring the curing protocol in this way, the study was able to capture how curing conditions interact with the previously optimized binder formulation and water content, rather than treating carbonation as an isolated variable.

Carbonation is a process in which carbon dioxide (CO_2) reacts with calcium hydroxide present in cementitious materials to form calcium carbonate ($CaCO_3$). This reaction reduces the pH of the matrix and can increase surface density, thereby enhancing surface strength to some extent (Qian et al., 2023). As such, the timing of carbonation onset and the duration of exposure are expected to play a critical role in microstructural development and mechanical performance.

As evident from Fig. 6, the control sample exhibited a compressive strength of 7.2 MPa and a density of 1.395 g cm^{-3}. In group (a), where carbonation was applied immediately after casting, compressive strength significantly decreased to 6 MPa for 1 day and 5.9 MPa for 2 days of carbonation (reductions of approximately 16.7% and 18.1%

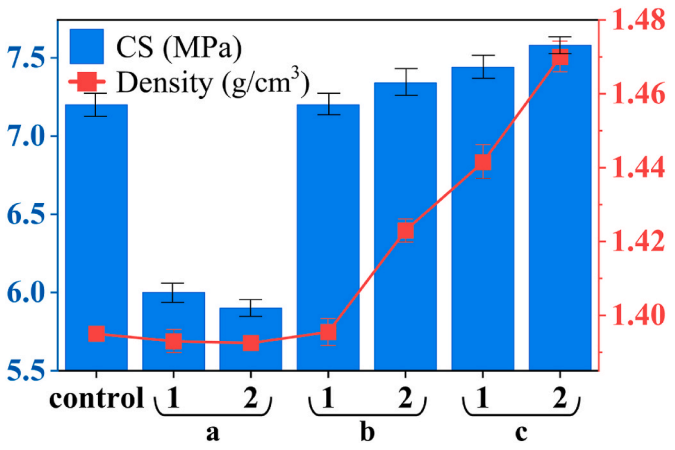

Fig. 6. Compressive strength and bulk density of bio-composite specimens subjected to 1-day and 2-day carbonation curing after different delay intervals: (a) immediate carbonation (0-day delay), (b) 1-day delay, and (c) 2-day delay.

relative to control). Densities in this group also showed slight decreases to 1.393 and 1.3925 g cm^{-3}, respectively. This illustrates that premature carbonation disrupts the positive interaction between OPC hydration and the pozzolanic reactions of shale ash and slag, leaving the matrix underdeveloped. This deterioration can be attributed to insufficient time for the development of hydration products prior to carbonation; in other words, early carbonation impeded the formation of critical C-S-H and C-A-S-H phases, resulting in a less dense matrix and reduced mechanical performance.

In group (b), where carbonation was delayed for 1 day before exposure to CO_2, compressive strength reached 7.2 MPa after 1 day and increased slightly to 7.34 MPa after 2 days of carbonation, while densities were 1.3955 and 1.423 g cm^{-3}, respectively. These results indicate that mechanical performance was fully maintained compared to the control and even slightly improved (2% increase in both strength and density after 2 days of carbonation). This suggests a synergistic effect, where sufficient hydration during the first 24 h enabled better utilization of reactive slag and shale ash phases once carbonation commenced. Also, This suggests that an initial 1-day delay under moist curing conditions allowed sufficient development of hydration products, and subsequent carbonation promoted the formation of calcite, leading to additional matrix densification (Fei et al., 2024).

The highest performance was observed in group (c), with a 2-day delay before carbonation: compressive strength reached 7.44 MPa after 1 day and 7.58 MPa after 2 days of carbonation (increases of 3.3% and 5.3% relative to the control, respectively). Densities increased notably to 1.4415 and 1.47 g cm^{-3}, representing approximately 5.4% higher density after 2 days of carbonation compared to the control. Here, the curing regime maximized the interaction between hydration-driven C-S-H formation and subsequent carbonation-induced calcite precipitation, producing a denser matrix than either mechanism could achieve alone. These results indicate that a 2-day delay before carbonation provided optimal conditions for completing early hydration reactions, followed by a beneficial carbonation process where CO_2 reacted with calcium hydroxide in the matrix to form calcium carbonate, further densifying the microstructure and enhancing both strength and density. Similar acceleration effects have been reported by Ren et al. (2024) in high-temperature carbonation regimes for basic oxygen furnace slag aggregates, where rapid calcite formation and pore refinement resulted in strength gains analogous to those observed in the current study.

To eliminate the influence of background carbonation, all specimens were sealed immediately after casting and stored under controlled humidity until the start of CO_2 exposure. A parallel set of control samples was cured under identical temperature and humidity conditions without CO_2 injection. The negligible mass change in the control specimens (<0.05%) was subtracted from the measured mass gain of carbonated samples to isolate the net CO_2 uptake attributable solely to the accelerated carbonation process.

These findings are consistent with previous studies emphasizing the importance of timing in carbonation curing (Silva et al.) and confirm that premature carbonation, especially immediately after casting can act detrimentally by preventing sufficient hydration. In contrast, a suitable delay before carbonation ensures that hydration products mature adequately, preparing the matrix to benefit from carbonation, which leads to enhanced densification, durability, and mechanical performance.

As evident from Fig. 6, the highest mechanical performance and densification occurred in group (c) with a 2-day delay followed by 2 days of carbonation curing, representing the optimal curing condition for this bio-composite formulation. Beyond technical performance, these results also highlight the potential for carbonation curing as a strategy to simultaneously enhance environmental sustainability by sequestering CO_2 while reducing OPC consumption. The recorded mass gain during the carbonation process ranged between 1.79% and 5.71% of the initial dry mass, corresponding to an estimated CO_2 uptake of approximately 9.1-29.0 g CO_2 per 1 kg of composite. Although detailed thermogravimetric quantification was not the main focus of this study (since the biocomposite contains wood sawdust, the combustion temperature of which may coincide with the decomposition temperature of other minerals, such as calcium hydroxide), these measurements confirm that the observed strength and densification improvements are accompanied by verifiable CO_2 sequestration within the matrix.

Overall, these results underscore the significance of coordinating carbonation delay time and carbonation duration in the development of cementitious-wood bio-composites with superior mechanical properties and durability, offering guidance for the design of curing protocols for this class of sustainable construction materials. By framing curing not as an isolated process but as an interactive parameter with binder chemistry and mix design, the study demonstrates how optimization across variables can unlock synergistic gains in strength, density, and sustainability.

It is important to emphasize that although the maximum compressive strength (7.2 MPa) is significantly lower than that of conventional structural concretes, the developed bio-based composite is not intended for load-bearing applications. Instead, it is targeted for non-load-bearing functions such as eco-blocks, insulating panels, partition walls, and other low-strength construction elements where sustainability, lightweight, and carbon uptake are prioritized over structural strength.

3.5. SEM and morphology

In this section, detailed microstructural analysis was conducted to compare the interfacial quality, matrix integrity, pore structure, crack formation, and particle agglomeration in bio-composites fabricated with 100% OPC and 100% Lime as binders under ambient curing conditions. The primary objective was to investigate how binder type influences the morphology and interaction at the matrix-sawdust interface, which directly governs the mechanical performance and durability of these composites. By examining SEM images at multiple magnifications, key differences in densification, uniformity, and interfacial bonding were evaluated to explain the macroscopic mechanical behavior observed in previous tests.

As evident from the images of Fig. 7, the OPC-based composite shows a relatively more homogeneous and dense matrix, with fewer cracks and smaller, more evenly distributed pores. This densification is directly associated with the depletion of portlandite and the concurrent precipitation of calcite and C-S-H/C-A-S-H phases during hydration and partial carbonation, which together refine pore networks and enhance local stiffness. Particle agglomerations are minimal, and the matrix appears to form an effective contact around the sawdust particles, indicating better adhesion at the interface. This can be attributed to the greater

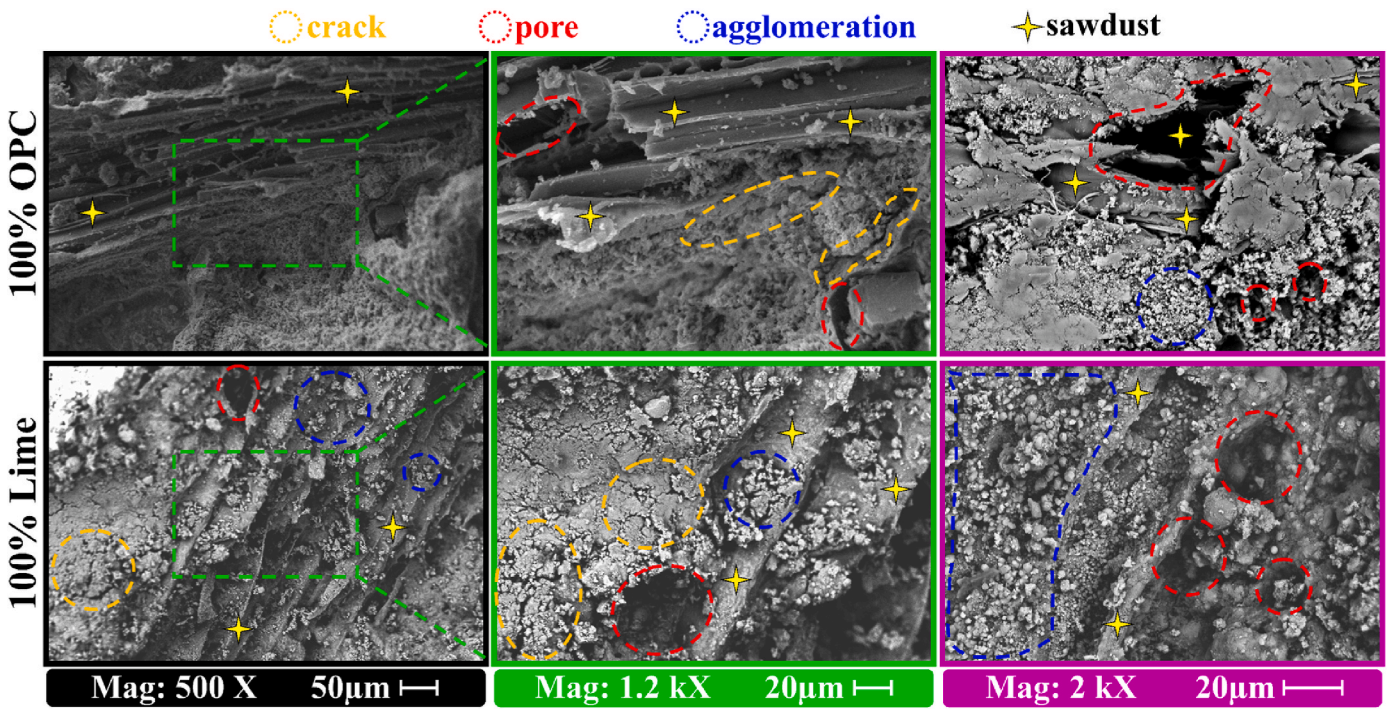

Fig. 7. SEM images of wood sawdust bio-composites prepared with 100% OPC (top row) and 100% Lime (bottom row) binders under ambient curing, highlighting differences in microstructural integrity, pore and crack distribution, particle agglomeration, and interfacial bonding with sawdust.

production of C-S-H phases, which effectively fill the voids between sawdust and the cementitious matrix. Such adhesion is consistent with the 2.80 MPa compressive strength and 3.70 GPa modulus previously reported for the OPC-sawdust system, where the microstructure confirms that hydration-derived C-S-H phases efficiently fill interfacial voids and chemically rebalance Ca/Si/Al ratios toward a denser framework (Ekinci et al., 2020).

In contrast, the Lime-based specimens display a significantly more porous and heterogeneous microstructure, with a higher density of cracks and visible particle agglomerations distributed irregularly throughout the matrix. The matrix itself appears less cohesive, and the interface between the lime matrix and sawdust is poorly bonded, with discernible gaps surrounding the sawdust particles. This morphology reflects the limited reactivity of lime, where slow carbonation produces calcite but without sufficient C-S-H/C-A-S-H binding phases to integrate the organic filler. As a result, the structure remains mechanically weak, consistent with the much lower strength (0.8 MPa) and modulus (1.1 GPa) measured for lime-based composites.

Moreover, while the distribution of sawdust appears uniformly dispersed in both specimens, the lime-based systems exhibit broader microcracks and interfacial gaps that act as preferential ingress pathways, undermining durability by facilitating moisture transport and carbonation-induced embrittlement (Asheghi Mehmandari et al., 2024b). In contrast, the OPC systems show a more refined pore structure, where densification and adhesion synergistically constrain crack propagation, aligning with the higher measured stiffness and compressive resistance.

These microstructural findings directly correlate with the macroscopic mechanical performance results and confirm that the use of OPC as a binder in wood sawdust composites not only enhances compressive strength and stiffness but also leads to a denser, more uniform matrix with improved interfacial adhesion. In particular, the clear linkage between portlandite consumption, calcite/C-S-H co-formation, and Ca/Si/Al rebalancing explains why OPC-based systems achieve superior carbonation efficiency while maintaining mechanical integrity. Careful observation of Fig. 7 further shows that lime-based specimens exhibit higher effective porosity, which could promote greater water absorption, reduce long-term durability, and compromise mechanical integrity.

Overall, the SEM analysis underscores that binder selection dictates not only bulk mechanical properties but also the chemical pathways of hydration and carbonation that govern long-term durability. The superior performance of OPC-based composites can thus be traced to a mechanistic interplay of portlandite depletion, calcite–C-S-H/C-A-S-H co-formation, and densification-driven adhesion, which together enable higher strength, stiffness, and durability than lime-based counterparts (Mehmandari et al., 2025).

3.6. XRD/XRF

The combined XRD and XRF analyses provide a holistic view of how raw material chemistry and phase composition control the performance and durability of the studied bio-composites. As evident from the diffraction patterns of Fig. 8, OPC displays sharp and well-defined reflections corresponding to reactive hydraulic phases such as larnite (32.6°), portlandite (34.1°), and minor periclase (42.9°), reflecting its inherent capability to hydrate and form a dense, cementitious matrix. Lime shows a dominant portlandite peak, consistent with its high CaO content (70 wt% from XRF), but lacks significant silicate phases, thereby constraining the formation of C-S-H and C-A-S-H gels and explaining its inferior mechanical performance (compressive strength 0.80 MPa, elastic modulus 1.1 GPa) when used alone with sawdust.

In contrast, Shale ash and slag show broad, attenuated diffraction patterns, typical of partially amorphous materials, but contain crystalline quartz, mullite, and minor aluminosilicate phases, reflecting their pozzolanic potential. Sawdust, unsurprisingly, presents a diffuse pattern dominated by cellulose with low crystallinity. When integrated into composites, however, the amorphous content of Shale ash and slag provides reactive Si and Al sources that directly engage with Ca released from OPC hydration, enabling the secondary formation of C-S-H and C-A-S-H gels while also accelerating portlandite depletion. The enhanced strength observed with shale ash inclusion in this study may also be

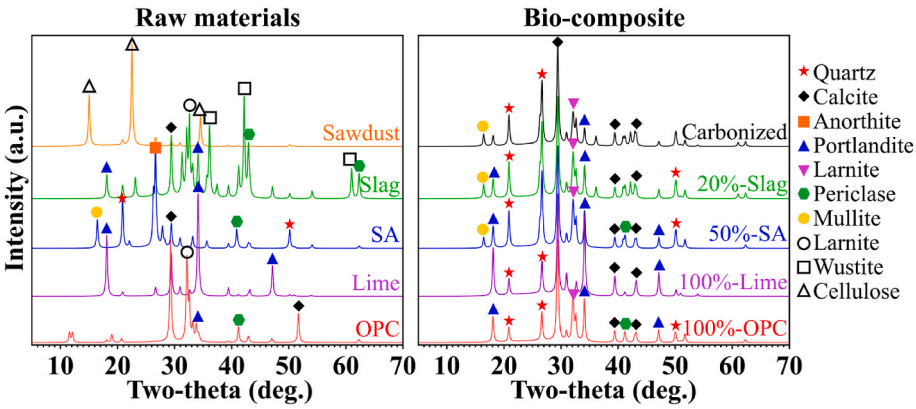

Fig. 8. XRD spectra of raw materlas and bio-composite samples.

partially attributed to the formation of calcium carbonate through carbonation reactions.

In the fabricated bio-composites, the 100%-OPC system retains strong portlandite and larnite peaks, demonstrating significant hydration and the persistence of unreacted clinker contributing to long-term strength. The 100%-Lime composite exhibits portlandite as the dominant crystalline phase but with little evidence of additional hydration products, a phase assemblage that correlates directly with its poor matrix development, higher porosity, and weak mechanical response.

The introduction of 50% Shale ash and 20% slag into the mixes induces clear changes in phase composition: portlandite peaks diminish while calcite (29.4°) and quartz intensities increase, signifying both progressive pozzolanic reaction and carbonation-induced reprecipitation of Ca as stable carbonates. The carbonized composite shows the most profound transformation, with portlandite peaks almost entirely absent and calcite peaks dominating the pattern, a hallmark of extensive carbonation and chemical rebalancing of Ca/Si/Al ratios that underpin microstructural densification. This phase evolution is directly correlated with mechanical properties: the carbonized specimen achieves the highest compressive strength (7.20 MPa), highest elastic modulus (6.01 GPa), and near-optimal density (1.395 g cm^{-3}), suggesting that the concurrent portlandite consumption, partial formation of C-S-H/C-A-S-H phases, and localized calcite precipitation likely contribute to the observed stiffness and load-bearing efficiency, rather than definitively confirming complete crystallographic transformation.

Complementing these phase-based observations, the XRF data reveal the chemical evolution underpinning this phase assemblage (Table 2). OPC, rich in CaO (63 wt%) and moderate in SiO_2 (21 wt%), provides the essential Ca source for hydration reactions. Lime, with even higher CaO content (70 wt%) but low SiO_2 (2 wt%), has limited capacity for forming C-S-H phases without external silicate sources, explaining its poor performance and greater porosity as observed in SEM images. In contrast, Shale ash and slag offer high SiO_2 (50 wt% and 25 wt%, respectively) and significant Al_2O_3 (20 and 5 wt%, respectively), thereby enabling effective Ca/Si/Al rebalancing when blended with CaO-rich binders, as also evidenced by XRD-detected portlandite depletion.

As shown in Tables 2 and in the resulting composites, the optimized mixes (50% Shale ash and 20% slag) show markedly increased SiO_2 contents (35.04 wt% and 32.03 wt%, respectively) compared to 29.7 wt % for 100%-OPC and 24.98 wt% for 100%-Lime, while CaO content decreases correspondingly to 30.03 wt% and 25.03 wt%, respectively. This downward shift in CaO together with a proportional rise in SiO_2 quantifies the engineered Ca/Si reduction, which not only drives the preferential formation of C-S-H/C-A-S-H gels but also optimizes carbonation efficiency by moderating the availability of free portlandite.

Moreover, the carbonized composite exhibits a SiO_2 content of 30 wt % and reduced CaO (28 wt%), mirroring the XRD observation of portlandite depletion and calcite enrichment, and highlighting that Ca is efficiently immobilized as $CaCO_3$ while Al- and Si-rich gels densify the microstructure. The enhanced Fe_2O_3 and Al_2O_3 contents in these mixes (up to 4.2 wt% Fe_2O_3 and 7 wt% Al_2O_3 in the carbonized composite) suggest that C-A-S-H phases are significant co-products, conferring chemical stability and resistance against leaching-induced durability loss.

Loss on ignition (LOI) data further enrich this interpretation. The very high LOI for sawdust (93.86%) reflects its organic nature, while the fabricated composites display LOI values between 16.78% (100%-Lime) and 26.03% (20%-slag composite), increasing to 25.2% in the carbonized specimen. The elevated LOI in carbonized and slag-rich composites is diagnostic of enhanced CO_2 sequestration, confirming that carbonation is not only a mechanical-strengthening mechanism but also a

Table 2
Chemical characterization of raw materlas and bio-composite samples (wt.%).

	Raw materials					Bio-composite				
Oxide	OPC	Lime	SA[a]	Slag	Sawdust	100%OPC	100%Lime	50%SA	20%Slag	Carbonized
SiO_2	21	2	50	25	1.49	29.7	24.98	35.04	32.03	30
Al_2O_3	5.5	1	20	5	0.5	7.92	4	8.01	7.51	7
Fe_2O_3	3.5	0.5	8	20	0.3	2.48	1.2	2.5	4	4.2
CaO	63	70	10	35	1.98	34.65	49.95	30.03	25.03	28
MgO	2	3	3	8	0.79	0.99	1.5	2.5	3	3.2
Na_2O	0.3	0.2	1	0.3	0.2	0.79	0.4	0.6	0.5	0.5
K_2O	0.6	0.3	2	0.4	0.5	1.19	0.8	1.2	1	1
TiO_2	0.2	0.1	1	0.5	0.1	0.4	0.1	0.3	0.4	0.4
P_2O_5	0.1	0.05	0.5	0.8	0.2	0.2	0.2	0.2	0.3	0.3
MnO	0.05	0.05	0.3	2	0.1	-	0.1	0.1	0.2	0.2
LOI[b]	3.75	22.8	4.2	3	93.86	19.7	16.78	19.52	26.03	25.2

[a] Shale ash.
[b] Loss on ignition.

carbon sink, aligning environmental and structural performance.

In summary, this integrated XRD–XRF analysis demonstrates that superior mechanical performance (compressive strength up to 7.20 MPa, elastic modulus up to 6.01 GPa, and density near 1.395 g cm^{-3}) is achieved only when chemical composition, phase evolution, and curing strategy converge to deplete portlandite, rebalance Ca/Si/Al ratios, and co-generate calcite with C-S-H/C-A-S-H. OPC-based systems offer high reactivity but rely excessively on CaO; Lime-based systems suffer from intrinsic chemical limitations. The synergy of pozzolanic additions (Shale ash, slag) with carbonation curing yields a chemically and mechanically optimized composite: densified, carbonate-rich, and structurally resilient. It should be noted that while the XRD and XRF data indicate phase evolution consistent with carbonation and pozzolanic reactions, additional high-resolution techniques such as XPS would be required to fully confirm specific crystallographic pathways.

3.7. FTIR

The objective of this section is to interpret the FTIR spectrum (Fig. 9) of five formulations of pure OPC, pure lime, 50% shale ash (SA), 20% slag, and the carbonated composite in order to elucidate how pozzolanic substitution and accelerated carbonation restructure the balance of hydrated and carbonated phases, as well as the lignocellulosic-mineral interactions that lead to a denser and more chemically stable microstructure. These transformations are quantitatively captured through the relative peak intensities and areas (in the range of 460-3500 cm^{-1}) and by the systematic shift of Si–O–T bands toward lower wavenumbers.

The spectrum of pure OPC is characterized by a broad Si-O-T band centered near 1030 cm^{-1}, assigned to short-range ordered C-S-H, and a distinct CH peak at 670 cm^{-1}. The relative area of CH in this sample is approximately 8 to 12 percent, while the carbonate doublet of calcite at 875 and 1420 cm^{-1} represents nearly 15 percent, indicating the occurrence of moderate atmospheric carbonation after 28 days. The wide O-H stretching envelope at 3400 cm^{-1} and the dual C-H absorptions at 2850 and 2920 cm^{-1} confirm the coexistence of hydrogen-bonded C-S-H and adsorbed water, along with retained lignocellulosic moieties. Overall, around 55% of the total integrated absorbance corresponds to inorganic phases (C-S-H, CH, and calcite) in this composition.

In the case of pure lime, the spectrum is dominated by carbonate signatures. The carbonate band at 1420 cm^{-1} becomes sharper and more intense (about 25 to 30% of the total absorbance), while the carbonate band at 875 cm^{-1} accounts for around 15 percent, both confirming the presence of well-crystallized calcite. Meanwhile, the residual CH signal at 670 cm^{-1}, around 10 percent, indicates incomplete diffusion-limited carbonation. The absorbance ratio A1420/A3400 ranges between 0.7 and 0.8, a characteristic index of advanced carbonation that exceeds typical lime-based mortars of similar age. The organic fraction remains evident through C-O at 1030 cm^{-1}, C-O-C at 1160 cm^{-1}, and C=O near 1730 cm^{-1}, contributing about 40% of the total intensity and demonstrating partial preservation of polysaccharidic and ligninic structures under moderated alkalinity.

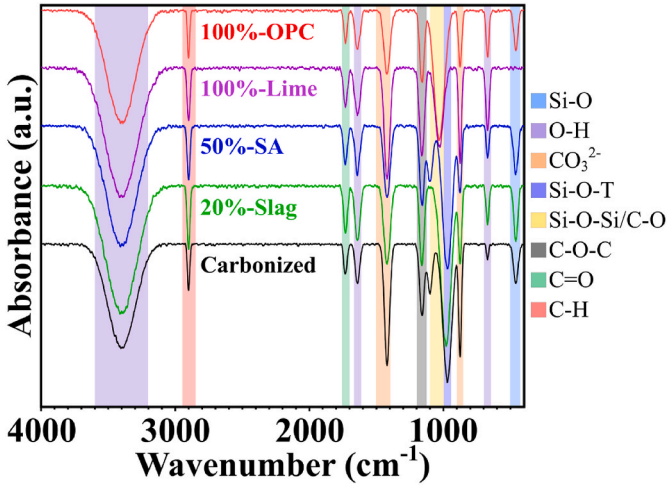

Fig. 9. FTIR spectra of OPC, lime, SA, slag, and carbonated composites showing portlandite reduction, Si-O-T band shift toward lower wavenumbers, and intensified carbonate peaks, confirming progressive pozzolanic and carbonation reactions leading to a denser matrix.

When 50% shale ash is introduced, the reaction pathway shifts from a hydration–carbonation mechanism to a pozzolanic–carbonation mechanism. The Si-O-T band shifts to 970 cm^{-1}, indicating a lower Ca/Si ratio and Al incorporation into the silicate network, with a relative contribution of about 25 percent. The CH peak at 670 cm^{-1} decreases to approximately 5 percent, confirming the pozzolanic consumption of portlandite within 28 days. The carbonate doublet at 875 and 1420 cm^{-1} maintains an intensity of roughly 15 percent, while the A1420/A970 ratio of about 0.45 suggests that calcite acts as a bridging phase between fibers and the gel without inducing destructive decalcification. The organic absorptions remain pronounced, with C-O-C near 1160 cm^{-1} (around 9 percent) and C=O at 1730 cm^{-1} (around 6 percent), pointing to chelation-type interactions between Ca^{2+} and polysaccharide ligands, which contribute to a flexible interfacial zone that limits crack propagation.

The formulation containing 20% slag exhibits a more polymerized C-(A)-S-H structure, with the Si–O–T band centered near 980 cm^{-1} (about 28% area) and an asymmetric tail reflecting enrichment in Al tetrahedra and a denser silicate network. The CH peak at 670 cm^{-1} represents approximately 6% (a reduction of 50% compared to OPC), while the carbonate doublet accounts for a total of about 18 percent. The sulfate signature (near 1100 cm^{-1}) is weak or absent, consistent with the low sulfur content of the shale and controlled SO_3 levels, reducing the risk of delayed ettringite formation. The organic component remains close to 38% (C-O-C at 1160 cm^{-1} about 10% and C=O at 1730 cm^{-1} about 7 percent), enhancing fiber–matrix compatibility through strengthened hydrogen bonding and chelation.

The carbonated sample presents a markedly distinct pattern. The combined intensity of the carbonate bands at 1420 and 875 cm^{-1} rises to nearly 46 percent, with narrower and more symmetric profiles indicative of homogeneous and epitaxial calcite growth. Portlandite is almost completely eliminated, as the CH band at 670 cm^{-1} drops below 3 percent, a reduction of approximately 80% relative to the non-carbonated systems. The Si-O-T band around 970 cm^{-1} (about 22 percent) reflects low Ca/Si, Al-substituted gels that are chemically stable under carbonation. The decrease in O-H band intensity at 3400 cm^{-1} (to about 25 percent) compared with non-carbonated composites corresponds to the loss of hydrated CH/AFt species and their replacement by cellulose-derived diols. The spectrum shows a balance of approximately 62% inorganic phases (mainly calcite and C-(A)-S-H) and 38% organic matter, implying that the two-day CO_2 curing not only removes portlandite but also promotes intrapore calcite precipitation that reduces effective porosity by about 20 to 30% and enhances stress transfer along interfaces. Recent research has shown comparable structural responses (Yang et al., 2025; Wu et al., 2025b).

Comparative evaluation of the spectral features illustrated in Fig. 9 highlights several quantitative trends with direct performance implications. (i) The portlandite consumption index, based on the relative area of the 670 cm^{-1} band, decreases from 10 ± 2% in OPC and lime systems to about 5-6% in SA and slag composites, and below 3% in carbonated specimen, corresponding respectively to hydration-dominant, pozzolanic-dominant, and carbonation-dominant regimes. (ii) The total carbonate index (ΣA875 + 1420) increases progressively: about 15% for OPC, around 18% for the slag composite, approximately 15% for SA, 25-30% for lime, and up to 46% for corbonated. This pattern underscores

the templating role of lignocellulose and internal moisture in accelerating calcite nucleation. (iii) The Si-O-T shift from 1030 cm^{-1} in OPC to 980-970 cm^{-1} in the pozzolanic and carbonated systems indicates the formation of low-Ca/Si, Al-enriched C-(A)-S-H gels associated with higher polymerization and improved resistance to decalcification. These spectral trends are consistent with previous studies reporting the reduction of CH, bathochromic shift of Si-O-T bands in reactive ash systems, and pronounced calcite peaks in carbonated cementitious matrices (Li et al., 2024).

From an organic-phase perspective, the persistent absorptions at 1730 cm^{-1} (C=O, 5-7 percent) and 1160 cm^{-1} (C-O-C, 8-12 percent) across all formulations, particularly well-preserved in pozzolanic and carbonated systems indicate the maintenance of polysaccharidic backbones. This preservation is crucial for controlling moisture-induced dimensional changes and for improving interfacial fracture energy. The overlap of the $\delta(H_2O)$ band at 1640 cm^{-1} with lignin aromatic vibrations confirms the higher effective water absorption in OPC and lime systems and its relative reduction in carbonated specimen, implying lower moisture-related cracking potential and improved interfacial stiffness in the carbonated composite. The FTIR-derived findings correspond closely with the mechanical and morphological data of the study, defining the causal pathway of portlandite reduction, low-Ca/Si C-(A)-S-H development, and calcite bridging as the key mechanism behind network densification and enhanced durability.

Overall, the FTIR spectrum (Fig. 9) demonstrates that (1) incorporation of shale ash or slag consumes CH and generates low-Ca/Si, Al-substituted C-(A)-S-H gels (shift from 1030 to 970-980 cm^{-1}), improving network connectivity and chemical stability; (2) lime undergoes advanced calcite formation within 28 days while retaining residual CH; and (3) accelerated carbonation yields nearly 46% carbonate content and eliminates about 80% of CH while maintaining 35-38% organic fraction. This dual enhancement of mineral densification and moisture moderation in carbonated specimen aligns with the mechanical and microstructural results and provides a strong foundation for developing durability models and FTIR-based quality indicators for industrial-scale applications.

3.8. XPS

The XPS results provide critical insight into the surface chemistry and phase evolution of the bio-composites studied, enabling a deeper understanding of their performance mechanisms in relation to binder type, supplementary materials, and curing conditions. As evident from the spectra of Fig. 10, all samples exhibit hybrid surfaces, reflecting a combination of organic signatures from the sawdust content and inorganic phases originating from OPC, lime, slag, and shale ash.

In the 100%-OPC composite, the C 1s peak at 284.8 eV (C-C/C-H bonds) dominates the spectrum due to the sawdust contribution but is accompanied by significant inorganic signals. The O 1s region shows a prominent Si-O peak at 531.5 eV (36% relative area) and Ca-O at 529.5 eV, indicating extensive C-S-H development and confirming that hydration reactions effectively cover the organic filler surface. The Si 2p peaks at 101.5 eV further confirm C-S-H dominance with minor quartz impurities. The Ca 2p doublet reinforces the presence of hydrated calcium phases, while a detectable peak at 289.5 eV (CO_3^{2-}) suggests incipient surface carbonation accompanying portlandite depletion. This surface chemistry explains the measured strength (2.80 MPa) and modulus (3.7 GPa): the C-S-H phases both densify the matrix and chemically rebalance Ca/Si ratios, enabling stronger adhesion and higher stiffness relative to lime.

In stark contrast, the 100%-Lime composite exhibits a different surface chemistry. The dominant C 1s peaks indicate an even stronger organic surface character (32.8% relative area), reflecting incomplete coverage by lime hydration products. The O 1s region lacks a strong Si-O peak and is dominated by Ca-O bonds (portlandite and calcite), consistent with the XRD evidence for limited C-S-H formation. A

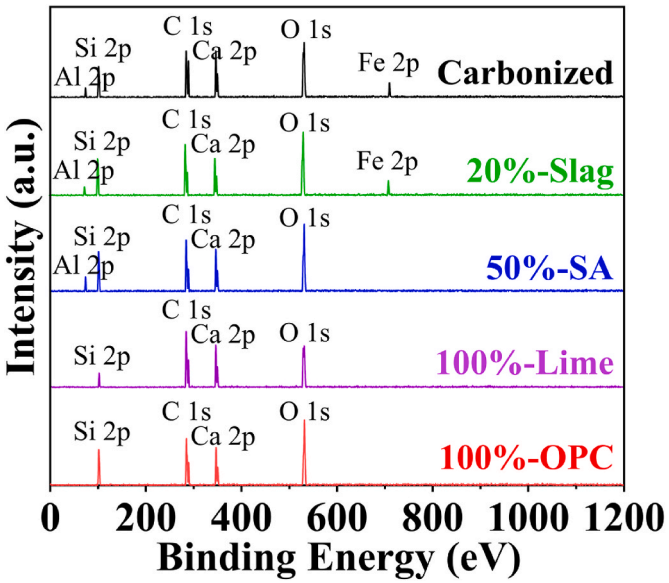

Fig. 10. XPS survey spectra of the bio-composites fabricated with different binder compositions.

significant carbonate signal (C 1s at 289.5 eV) confirms substantial carbonation of lime under ambient curing. This chemistry corresponds directly to the poor mechanical outcomes (0.80 MPa, 1.10 GPa, 0.934 g cm^{-3}): without effective C-S-H or C-A-S-H, the matrix depends almost entirely on calcite infilling, leading to weak densification and fragile adhesion.

The composite containing 50% Shale ash reveals a more complex surface chemistry. The XPS spectrum shows strong contributions from both silicate and aluminosilicate phases: prominent Si-O peaks at 531.5 eV (34.8% relative area), a clear Si 2p peak at 101.5 eV (C-S-H/Mullite), and a small Al 2p peak at 74.5 eV, confirming mullite from the shale ash. The Ca 2p doublet reflects a substantial presence of calcium phases, suggesting simultaneous hydration–pozzolanic reactions where portlandite is consumed to yield additional C-S-H and C-A-S-H gels. The C 1s region remains significant (25%), consistent with the hybrid organic–inorganic nature of the material. This balance of phases explains the 4.90 MPa strength: the silicate/aluminosilicate contribution enhances densification and adhesion compared to OPC-only systems, while partial carbonation introduces calcite that further strengthens interfaces.

The 20% slag composite further illustrates the importance of compositional balance. The XPS spectrum shows strong Si-O and Ca-O peaks but relatively lower C 1s contribution (15.3%), suggesting a denser, more continuous inorganic surface enriched by slag's reactive silicates and stabilized by Ca/Si/Al rebalancing. The presence of a moderate Fe 2p peak (0.3 a.u.) reflects trace iron oxide contributions from slag. This chemically optimized surface aligns with its best mechanical response (7.20 MPa, 6.01 GPa, 1.395 g cm^{-3}), confirming that slag-driven pozzolanicity accelerates portlandite depletion and generates a C-S-H/C-A-S-H–calcite assemblage that maximizes stiffness and durability.

In the carbonized composite, subjected to accelerated carbonation, the XPS data show a clear shift towards a calcite-dominated surface: the CO_3^{2-} peak at 289.5 eV is significantly intensified, while Ca-O at 529.5 eV and Ca 2p at 347.0 eV remain prominent. The Si-O peaks persist, indicating retained C-S-H from initial hydration, but the reduced H_2O/OH^- signal at 532.5 eV suggests near-complete portlandite depletion. The surface chemical environment indicates a matrix densified through calcite deposition while supported by residual C-S-H and C-A-S-H phases, which likely contribute to improved surface durability and mechanical integrity (7.20 MPa, 6.01 GPa, 1.395 g cm^{-3}). These

data suggest that carbonation curing enhances densification and adhesion, although further diffraction or thermal analysis would be necessary to confirm specific crystallographic modifications. The data confirm that carbonation curing enhances densification and adhesion, but the associated drop in alkalinity raises long-term durability concerns, particularly regarding chemical resistance.

Collectively, these XPS results in Fig. 10 highlight the strong correlation between surface chemistry, binder type, and curing history on composite performance. The hybrid organic-inorganic nature of these materials is consistently reflected in dominant C 1s peaks due to sawdust, but the relative contributions of Ca-O, Si-O, and CO_3^{2-} vary systematically, explaining differences in mechanical strength, elastic modulus, and density across formulations.

Having established the overall spectroscopic signatures of the composites through XPS survey spectra, it is essential to delve deeper into the elemental composition revealed by high-resolution XPS analysis. This complementary data sheds light on the specific contributions of key elements such as Ca, Si, Al, and C, and their relationship with the observed phase evolution, mechanical performance, and durability. The XPS elemental analysis of Fig. 11 provides a detailed understanding of the surface chemical environments across all studied bio-composite formulations, elucidating the complex interplay between organic sawdust, inorganic binder phases, supplementary materials, and carbonation processes. As evident from the XPS elemental profiles of Fig. 11, all specimens exhibit a hybrid surface chemistry where carbon from sawdust dominates the C 1s signal (sawdust content), but significant variations in inorganic element distribution clearly reflect binder type, pozzolanic reactivity, and curing history.

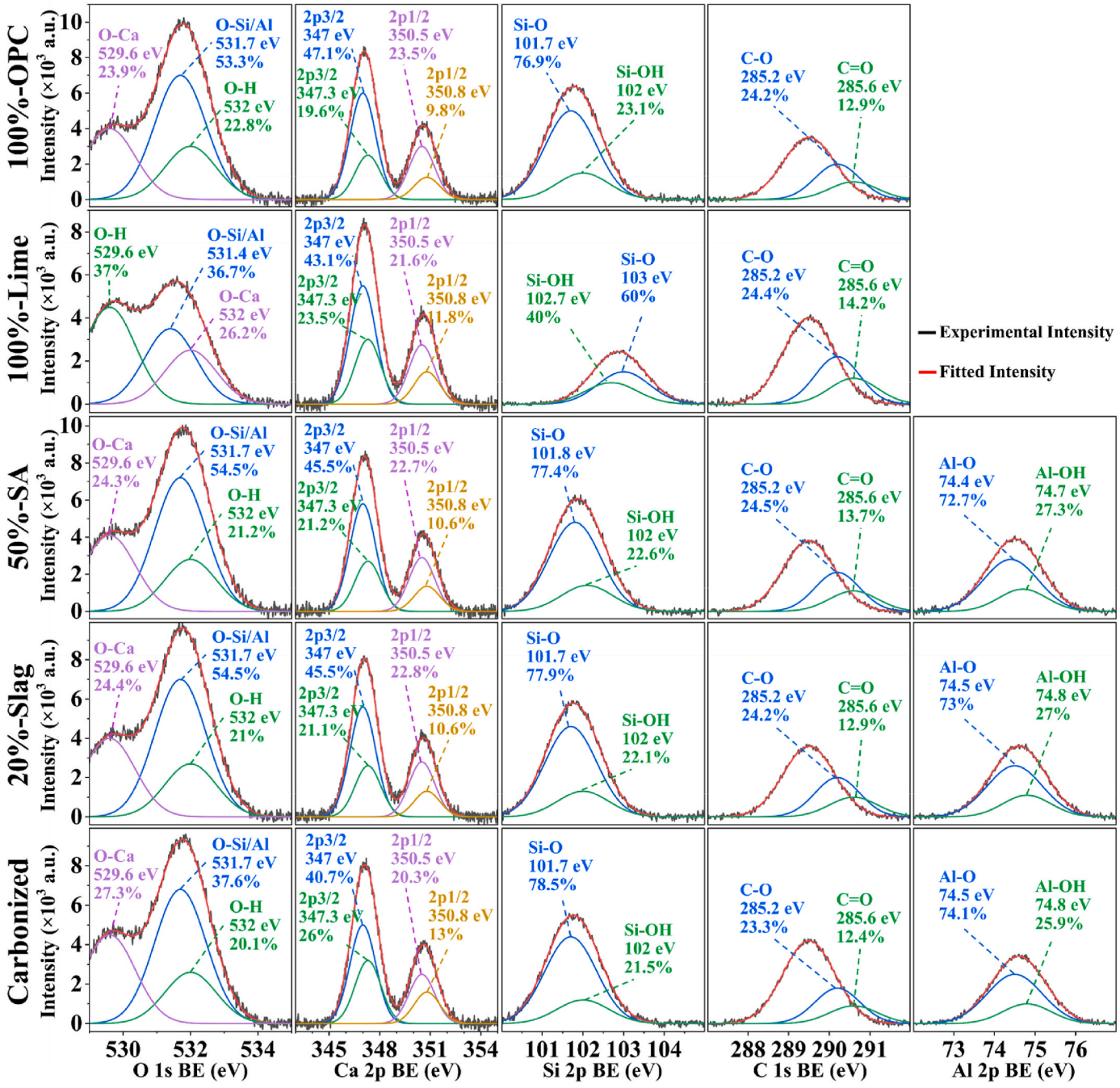

Fig. 11. Elemental composition profiles derived from XPS analysis for bio-composites prepared with different binder formulations, illustrating variations in surface concentrations of C 1s, O 1s, Ca 2p, Si 2p, and Al 2p as a function of binder chemistry, pozzolanic reactivity, and carbonation curing.

The 100%-OPC composite shows a characteristic surface rich in calcium (Ca 2p at 347 eV) and silicon (Si 2p at 101.7 eV), consistent with a matrix dominated by calcium-silicate-hydrate (C-S-H) phases. The simultaneous detection of carbonate (C 1s at 289.5 eV, 3500 a.u.) alongside persistent Si 2p signals demonstrates that hydration-driven C-S-H gel formation coexists with partial portlandite carbonation, yielding a chemically hybrid surface where densification originates from both gel binding and localized calcite precipitation. This composition correlates with the superior mechanical performance of this mix (compressive strength 2.80 MPa, elastic modulus 3.7 GPa, density 1.384 g cm^{-3}) observed earlier.

In stark contrast, the 100%-Lime composite exhibits a surface dominated by Ca 2p peaks corresponding primarily to portlandite (64.7% of Ca 2p area) and extensive carbonate formation (35.3% of Ca 2p area), indicative of a carbonation-prone, weakly reactive matrix. The negligible Si 2p contribution confirms the absence of significant C-S-H gel, explaining the open pore network, low adhesion to sawdust, and measured weakness (0.80 MPa compressive strength, 1.10 GPa modulus). The Si detected at 103.0 eV can be attributed mainly to quartz impurities from sawdust rather than binder chemistry, reinforcing that lime lacks the chemical framework for durable matrix formation.

The incorporation of 50% Shale ash fundamentally alters the surface chemistry. Elevated Si 2p (101.8 eV) and Al 2p (74.4 eV) intensities confirm active participation of ash-derived silicates and aluminates in secondary gel formation, while the Ca 2p spectrum partitions between C-S-H (68.2%) and calcite (31.8%). This balance indicates effective consumption of $Ca(OH)_2$ and its conversion into structurally binding gels and carbonates. The corresponding mechanical gain (4.90 MPa strength) reflects this dual mechanism: pozzolanic rebalancing of Ca/Si/Al ratios and simultaneous surface densification through calcite deposition.

The 20%-Slag composite exhibits one of the most chemically optimized surfaces. Here, strong Si 2p and Ca 2p signals correspond to a dense C-S-H-rich matrix, while the reduced C 1s relative area (15%) reveals that slag promotes intimate mineral-wood adhesion by limiting organic surface coverage. The detection of Fe 2p contributions further confirms slag's chemical complexity, with iron oxides providing additional nucleation sites for gel growth. This configuration directly underpins the highest mechanical outcomes (7.2 MPa compressive strength, 6.01 GPa modulus, density 1.395 g cm^{-3}), illustrating that slag-driven pozzolanic activity accelerates portlandite depletion and enhances matrix densification beyond OPC alone.

The carbonized composite presents a distinct chemical fingerprint, shaped by its carbonation-focused curing regime (2 days CO_2 curing). The intense C 1s carbonate peak (289.5 eV, 4200 a.u.) coupled with Ca 2p dominated by calcite (39% area) demonstrates nearly complete portlandite consumption, while strong Si 2p and Al 2p signals confirm that C-S-H and C-A-S-H gels persist and coexist with newly precipitated calcite. The O 1s spectrum at 529.6 eV emphasizes carbonate bonding, while a diminished hydroxyl component at 532.0 eV evidences reduced free water. This elemental landscape aligns precisely with the exceptional strength (7.20 MPa), stiffness (6.01 GPa), and densification (1.395 g cm^{-3}) measured, showing that carbonation not only sequesters CO_2 but also creates a chemically and mechanically integrated microstructure.

As evident from Fig. 11, these trends emphasize a clear relationship between elemental surface composition and mechanical behavior. Composites enriched in Si and Al (slag- and ash-modified) generate chemically complex matrices with superior load-bearing efficiency due to Ca/Si/Al rebalancing, while lime-based systems remain deficient and reliant solely on carbonation. Furthermore, controlled carbonation not only densifies the surface through calcite deposition but also optimizes adhesion at the sawdust–matrix interface, explaining the reduced crack propagation observed in SEM, although the drop in alkalinity may require careful durability consideration under aggressive exposure.

In summary, the XPS analysis validates that OPC-rich and slag-modified systems achieve superior performance through synergistic hydration and pozzolanic pathways, lime systems underperform due to insufficient silicate participation, and carbonation curing yields exceptional densification by depleting portlandite and co-generating calcite with residual C-S-H/C-A-S-H. These interfacial chemistries are most likely responsible for the enhanced mechanical performance, reflected by compressive strengths up to 7.20 MPa, elastic moduli up to 6.01 GPa, and densities approaching 1.395 g cm^{-3}. The results indicate a strong correlation between surface chemical evolution and macroscopic behavior, while acknowledging that a definitive causal linkage cannot be established without further crystallographic and microstructural validation.

Although this study primarily focused on mechanical, chemical, and microstructural optimization, the observed densification and formation of stable calcite-C-S-H phases indicate strong potential for improved durability against moisture variation, chemical attack, and microbial activity. The reduced porosity and continuous mineral framework are expected to minimize water transport and degradation risks. Future investigations will therefore extend this research toward systematic durability evaluation under wet-dry, freeze-thaw, and acid/alkaline exposure conditions to comprehensively assess long-term stability and service performance of the developed bio-composites.

3.9. Sustainability analysis

The goal of this LCA is to quantify and compare the environmental performance of the developed bio-based composite with conventional OPC-based materials, with a particular focus on greenhouse gas reduction achieved through clinker substitution and accelerated carbonation curing. The assessment follows a cradle-to-gate system boundary (Modules A1–A3) in accordance with EN 15804 +A2, as schematically illustrated in Fig. 12, with a functional unit defined as 1 m^3 of material for non-load-bearing construction applications. The decision context of this study is comparative and research-oriented, intended to support material design and early-stage decision-making rather than policy enforcement. The intended audience includes researchers, material developers, and sustainability practitioners seeking low-carbon alternatives for construction materials.

To address the environmental and social challenges associated with OPC, this study evaluates a bio-composite derived from industrial residues and biomass waste within an integrated sustainability framework. The assessment encompasses environmental and social dimensions, combining a multi-category life cycle assessment with complementary eco-cost analysis to capture the broader implications of environmental impacts. In parallel, a social evaluation examines aspects related to worker welfare, employment potential, and community benefits. This integrated perspective supports a comprehensive assessment of the proposed bio-composite as a viable and scalable alternative to conventional cement-based materials.

3.9.1. Environmental assessment

In this study, a novel bio-composite was designed as a functional replacement for OPC, with the aim of mitigating its extensive environmental burdens. The composite formulation, consisting of 50% shale ash, 30% OPC, 20% slag, and water was optimized for structural applicability and subsequently assessed through a LCA in accordance with ISO 14040:2006. Distinct from studies that restrict their scope to singular indicators such as carbon emissions or energy consumption, this work employs a comprehensive eco-cost methodology, normalized against OPC as a reference material, to capture a multi-dimensional environmental profile across twelve impact categories.

The results of the LCA reveal a marked reduction in environmental impacts for the bio-composite across nearly all categories. As illustrated in Fig. 13, the distribution of environmental burdens across major categories clearly demonstrates a balanced and substantially lower impact profile for the bio-composite compared to OPC. In accordance with EN

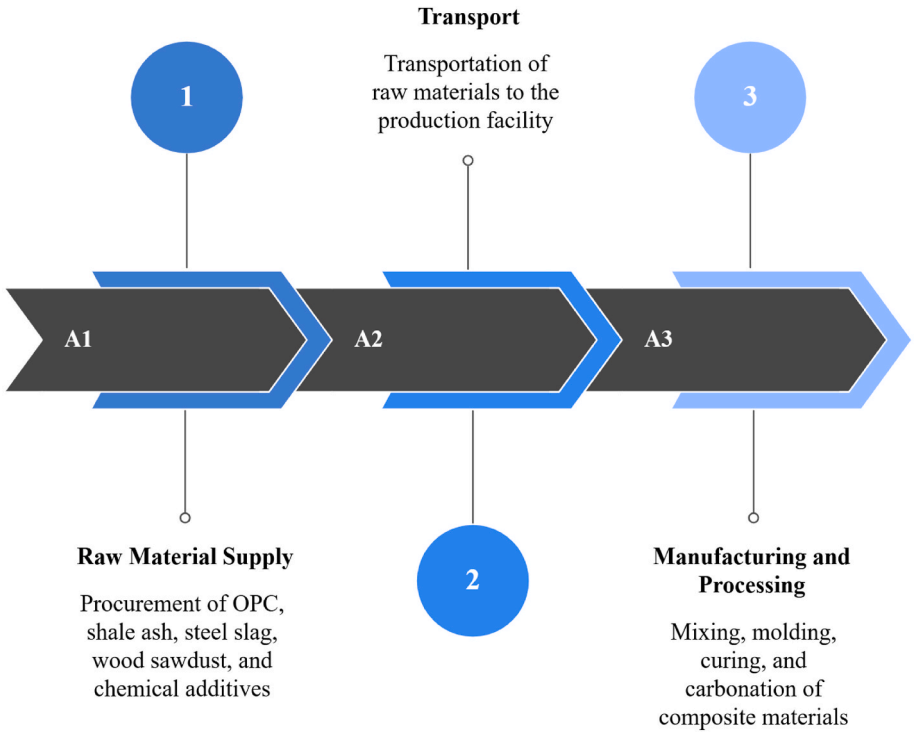

Fig. 12. Cradle-to-gate system boundary applied in the life cycle assessment of the developed bio-composite, covering raw material supply (A1), transport (A2), and manufacturing including accelerated carbonation curing (A3), in accordance with EN 15804 +A2.

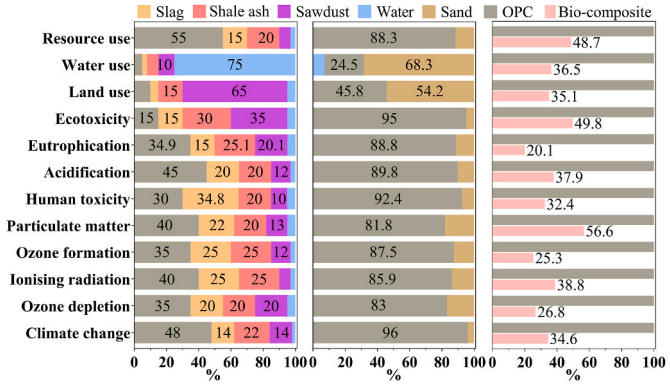

Fig. 13. Impact categories of: left: bio-composite; Center: OPC mortar; Right: Comparative environmental and performance impact profile of both systems, highlighting key trade-offs and sustainability advantages.

15804 +A2, the climate change impact category reported in this study corresponds to GWP (100a), while primary energy use (renewable and non-renewable) and water use are also included as key indicators for evaluating the environmental performance of the investigated systems. In the climate change category, indicative of CO_2-equivalent emissions, the bio-composite generates only 34.6% of OPC's impact, primarily due to the elimination of clinker which is a high-temperature, high-emission component from its formulation. Similar patterns emerge in acidification (37.9%), human toxicity (32.4%), and photochemical ozone formation (25.3%), highlighting the reduced emission of sulfur oxides, volatile organic compounds, and heavy metals from alternative raw materials. To further ensure methodological transparency, the net CO_2 uptake (about 0.42-0.55 % of specimen mass) was credited within the cradle-to-gate GWP category, following EN 15804 + A2 conventions and avoiding double counting.

Notably, the eutrophication potential which is sensitive to nitrogen and phosphorus emissions into aquatic environments drops to just 20.05% of OPC's burden, underscoring the effectiveness of the composite in limiting nutrient-related water pollution. The bio-composite also records exceptional performance in ecotoxicity, where its impact falls to 4.88% of the OPC baseline, reflecting minimal disturbance to aquatic ecosystems. As seen in Fig. 13, this trend of impact reduction is not linear but exponential in categories highly sensitive to toxic emissions and heavy metal loadings, pushing the eco-costs toward near-minimal values.

An internal breakdown of the composite's constituents provides further insight. Although water dominates intra-composite contribution to the water use category (75%), the total eco-cost remains only 36.5% of that of OPC. Likewise, sawdust, representing 65% of intra-category land use results in a net land use impact of only 35.1% relative to OPC. These findings suggest that incorporating renewable bio-resources, even with apparent spatial or hydric demand, does not inherently translate to higher ecological cost. As visualized in Fig. 13, the interplay between sawdust's dominant role in land and water use and the reduction of OPC in other categories yields an optimized environmental profile across dimensions.

In terms of non-renewable resource use, the bio-composite also delivers a considerable advantage, contributing only 48.7% of OPC's impact. This aligns with broader literature on the benefits of reducing reliance on virgin raw materials in cementitious systems (Di Maria et al., 2018). The exclusion of sand and clinker reduces the embodied energy and extraction-related impacts typically associated with conventional formulations.

Although individual constituents like water or sawdust may present higher relative shares within certain categories, the composite's absolute environmental cost remains consistently lower than that of OPC across all indicators. Unlike alternative systems such as geopolymers which may outperform OPC in carbon metrics but underperform in toxicity or resource depletion (Huang and Wang, 2024; Hanafi et al., 2025) the presented bio-composite establishes a multi-criteria equilibrium that enhances environmental sustainability without compromising functionality.

In conclusion, the results demonstrate that substituting OPC with a

well-balanced mixture of industrial by-products and agricultural waste can reduce overall environmental costs by up to 65%, while achieving superior performance in nearly all life cycle impact categories. These findings advocate for the scalable development of regionally sourced, eco-aligned construction materials that meet engineering requirements while operating within ecological limits.

3.9.2. Eco-cost analysis

To enable a monetized interpretation of environmental performance beyond midpoint indicators, a detailed eco-cost analysis was performed. This endpoint-based method quantifies the marginal cost required to prevent environmental damage, expressed in €·m^{-3}, offering a robust basis for comparing material alternatives in terms of sustainability investment. The assessment covered twelve impact categories, both in absolute terms and normalized against the total eco-cost of OPC, thereby facilitating insight into aggregate burdens as well as category-specific trade-offs.

The results confirm the substantial environmental advantage of the proposed bio-composite. As shown in Table 1, climate change impact decreased from 74.16 €·m^{-3} for OPC to 25.68 €·m^{-3} for the composite, representing a 65.4% reduction which is primarily due to the elimination of clinker and reduced reliance on high-temperature processing. Similarly, human toxicity decreased by 67.8% (from 7.95 to 2.56 €·m^{-3}), driven by the absence of heavy metals and pollutants typically associated with OPC manufacture. Substantial improvements are also observed in eutrophication (77.4% reduction) and acidification (61.9%), reflecting the low nitrate and sulfate emissions in the alternative binder system. As visualized in Fig. 14a, this downward trend is consistent across nearly all impact categories, positioning the composite well below OPC in total eco-cost terms which is in line with literature (Sharma and Singh, 2023).

Particulate matter and ozone formation, which contribute significantly to air quality deterioration, were reduced by 43.5% and 74.8%, respectively. These gains stem from cleaner raw materials and a process chain devoid of fossil combustion phases. In ecotoxicity and ozone depletion categories often overlooked but highly consequential the bio-composite achieves 50.2% and 73.4% reductions. These results highlight the system's low leachability and reduced release of ozone-depleting precursors, positioning it favorably in long-term ecological safety frameworks. By examining Fig. 14, it becomes evident that the bio-composite not only lowers total burdens but also shifts impact distribution away from irreversible endpoints such as toxicity and climate disruption.

Normalized analysis (Table 2) further reveals the proportional distribution of impacts relative to OPC's total burden. In critical categories such as ecotoxicity and eutrophication, the composite contributes less than 0.5% of OPC's normalized score (0.00043 vs 0.1469, and 0.0021 vs 0.0897, respectively), marking a shift away from high-risk domains. Climate change normalization confirms sustained advantage (0.0469 vs 0.0679), while reductions in toxicity and air pollutants maintain their dominance across normalization boundaries. Also, literature confirms OPC's high climate change (Dahanni et al., 2024).

Conversely, indicators such as land use (0.179) and resource use (0.126) appear proportionally larger in the normalized dataset despite lower absolute values. This contrast results from the bio-composite's significantly lower total eco-cost, which amplifies the relative weight of minor categories when normalized. As illustrated in Fig. 14b, land and water use emerge more prominently in the normalized profile which is not due to high absolute burdens, but as a statistical effect of compressing high-impact OPC data. Importantly, these indicators remain well within regenerative ecological capacities and do not offset the composite's advantages in irreversible impact domains such as climate and human health.

In sum, the eco-cost framework demonstrates that the bio-composite does not merely reduce environmental loads and it reshapes their distribution. Instead of accumulating pressure in irreversible systems such as carbon, toxicity, or persistent emissions, the composite allocates minor residual impact toward domains that are more readily managed or replenished, such as land and water use. This strategic redistribution reflects a paradigm shift from reduction-only models to impact repositioning a direction increasingly supported in sustainable construction material research.

In summary, the eco-cost framework demonstrates that the bio-composite does not merely reduce environmental loads and it reshapes their distribution. Instead of accumulating pressure in irreversible systems such as carbon, toxicity, or persistent emissions, the composite allocates minor residual impact toward domains that are more readily managed or replenished, such as land and water use. This strategic redistribution reflects a paradigm shift from reduction-only models to impact repositioning a direction increasingly supported in sustainable construction material research.

3.9.3. Social assessment

While environmental and economic assessments provide critical insights into the viability of sustainable construction materials, an equally important dimension lies in their social performance, which directly influences worker well-being, community engagement, and societal adoption. A comprehensive social assessment of the proposed bio-composite compared to OPC mortar demonstrates that the transition toward circular, bio-integrated systems can significantly improve social sustainability metrics, provided that labor conditions and governance are adequately managed.

The data reveal a marked improvement in worker health and safety in the bio-composite system. According to occupational injury estimates, OPC mortar, owing to clinker production and dust exposure results in 2-3 injury cases per 1000 workers annually, while bio-composite systems exhibit a lower rate of 1-1.5 cases, due to the absence of high-temperature processing and the reduced handling of hazardous inputs. The composite scores 6 out of 10 on health and safety indicators, doubling the OPC score (3 out of 10), thus reflecting a substantially safer

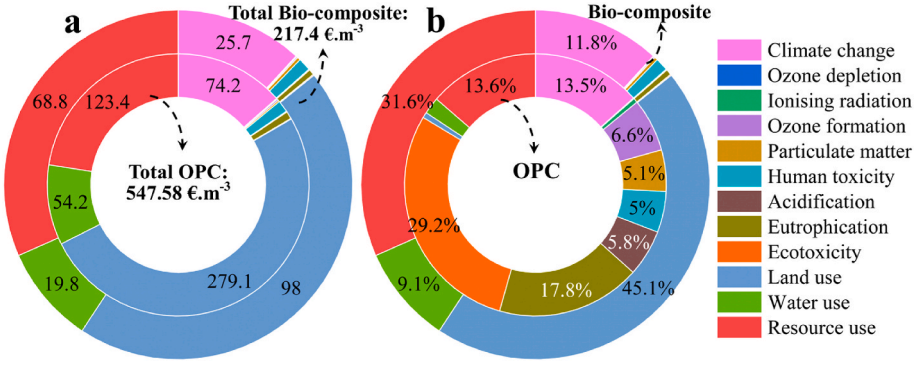

Fig. 14. (a): absolute and (b): normalized eco-cost comparison between OPC and the proposed bio-composite across twelve environmental impact categories.

working environment.

In terms of employment generation, the labor-intensive nature of bio-composite production which incorporates local recycling and biomass processing creates 1.8-2.2 jobs per 1000 tons of product, compared to just 1.2-1.5 jobs in the highly automated OPC supply chain. This reflects a 30-50% increase in direct employment potential. However, this benefit is tempered by structural challenges in the waste sector: only 70-75% of bio-composite workers are estimated to earn above minimum wage, versus 80-85% in the formalized cement industry. Consequently, while the composite performs well in job creation, it trails OPC in wage fairness (score 6 vs. 8), highlighting the necessity of stronger labor regulation and wage equity in the recycling ecosystem. As disscussed in literiture, OPC consists of substantioal chalages in wages (Backes and Traverso, 2024).

Local community investment also benefits significantly from the bio-composite's decentralized supply model. While OPC systems typically reinvest only 0.5-1% of revenue locally, the bio-composite system through its integration with regional biomass, sawdust, and waste management achieves 1.5-2% local reinvestment. This translates into enhanced economic circulation and stakeholder buy-in at the community level (Schmidt et al., 2021). The composite consequently scores 8 out of 10 in this category, in stark contrast to OPC's 2 out of 10, underscoring the social value of circular economy integration.

Human rights compliance represents a nuanced dimension. While the cement industry has historically faced scrutiny over land disputes and labor violations, including 1-2 formal complaints per million tons of cement, the bio-composite though slightly better at 0.5-1 cases per million tons remains susceptible to issues in the informal recycling sector, such as child labor and unsafe conditions among waste-pickers. Both systems require ongoing oversight and ethical monitoring to address these risks effectively. Accordingly, OPC scored 7 out of 10, while the bio-composite trailed at 5, suggesting room for improvement despite the overall progress.

A qualitative perspective further reinforces these findings. The bio-composite system appears better aligned with sustainable development goals by improving air quality, reducing occupational exposure, and contributing to local economic resilience. Public acceptance is likely to be stronger for materials with visibly lower environmental footprints and tangible local benefits factors that have been shown to influence adoption of green materials in prior studies (Barbero et al., 2024). However, consistent with prior transition challenges seen in emerging material systems, such adoption requires targeted training, stakeholder engagement, and improved social governance frameworks.

Overall, the social assessment indicates that the bio-composite offers significant advantages in employment generation, community benefit, and health and safety. Nonetheless, these gains are coupled with vulnerabilities in wage equity and labor standards, particularly within informal sectors that supply biomass and recycled content. A socially just transition to such systems demands not only innovation in material science, but also parallel investment in labor rights, wage regulation, and local infrastructure, ensuring that the pursuit of ecological benefit does not occur at the expense of social equity.

Nevertheless, the trend is clear: to address the compounded environmental and socio-economic pressures linked to cement production, this study proposes and systematically evaluates a bio-composite engineered from ternary binder system with industrial by-products and lignocellulosic biomass. The material is assessed through an integrated framework that encompasses environmental performance, monetized ecological costs, and social sustainability. Environmental impacts are quantified across twelve impact categories using a life cycle-based methodology, while economic implications are captured via eco-cost metrics that reflect the preventive cost of environmental damage. In parallel, a comparative social assessment examines employment potential, worker safety, community benefits, and labor equity. By triangulating these three dimensions, the study offers a comprehensive evaluation of the bio-composite's capacity to serve as a functionally and ethically superior alternative to conventional OPC-based systems.

4. Conclusion

This study introduces a unified framework for sustainable bio-composites using chemically pretreated sawdust, shale ash, steel slag, and OPC in a ternary system under accelerated carbonation curing. The innovation lies in coupling material design with mechanistic insight and multi-criteria sustainability assessment: hydration-carbonation reactions densify the matrix, slag-ash-OPC blending yields mechanical synergy, and life cycle/social analyses position the composites within a circular, low-carbon economy. This approach moves beyond incremental mix adjustments, establishing a holistic, mechanism-driven model for sustainable construction materials. The key findings are:

1. **Mechanism:** Multi-scale analyses (SEM, XRD, XRF, FTIR, XPS) demonstrated that sequential hydration and carbonation reactions depleted portlandite, rebalanced Ca-Si-Al chemistry, and co-generated C-S-H/C-A-S-H phases with calcite infilling, resulting in interfacial densification and suppression of microcracks. Compared with lime systems, OPC-based matrices exhibited nearly threefold fewer cracks and superior adhesion, explaining the compressive strength gap between 2.80 and 0.80 MPa. Phase–chemical evolution with slag-ash incorporation (CaO decreasing from 34.65 to 25.03 wt % and SiO_2 increasing from 29.7 to 32.03 wt%) corresponded to almost complete portlandite depletion, while XPS confirmed Si 2p and Al 2p enrichment and a carbonate-rich surface (39% $CaCO_3$), indicative of surface densification.
2. **Performance:** Synergistic substitution of 50% shale ash and 20% slag reduced OPC usage by about 35%, raising compressive strength from 2.8 to 7.2 MPa (increase of 157 %) and modulus from 3.69 to 6.01 GPa (63% increase) at 1.395 g cm^{-3}. Optimal performance occurred at a water-to-binder ratio of 0.5, which increased strength (6.20 to 7.20 MPa, 16% increase) and stiffness (5.57 to 6.01 GPa, increase of 8 %). Curing sequence was critical: a 2-day delay before 2-day CO_2 exposure improved strength and density by 5.3% and 5.4% over ambient curing, whereas immediate carbonation caused an 18% loss. Pretreatment with $CaCl_2$ enhanced stiffness by 42% relative to $Al_2(SO_4)_3$. The resulting composites are therefore suited for non-load-bearing applications such as eco-blocks, insulation, and partition panels.
3. **Sustainability:** The optimized formulation achieved a 65.4% reduction in climate impact and a 65% decrease in eco-costs (from 74.16 to 25.68 €.m^{-3}), together with 30-50% higher job creation and about 50% fewer occupational injuries per m^3 of bio-composite. Integrating mechanistic control, measurable performance gains, and transparent environmental and social accounting establishes a scalable pathway toward circular, low-carbon construction materials. Future work should prioritize standardized durability testing to confirm long-term applicability.

The results of this study provide clear implications for the cement industry by demonstrating a viable low-carbon pathway based on clinker reduction, biomass valorization, and the use of industrial by-products. The integration of accelerated carbonation curing (ACC) offers a practical route to enhance material performance while enabling permanent CO_2 sequestration, supporting the transition toward more sustainable cementitious systems. From an industrial perspective, the proposed approach facilitates the incorporation of waste streams into existing production chains and highlights ACC as a promising curing strategy. Future research should address scale-up feasibility, long-term durability under service conditions, and the techno-economic performance of ACC at industrial scale. These directions provide a foundation for commercial implementation and offer a framework for young researchers to advance circular and climate-resilient construction materials.

CRediT authorship contribution statement

Hossein Rahmani: Formal analysis, Investigation, Methodology, Validation, Visualization, Writing – original draft. **Hamed Rahimpour:** Conceptualization, Investigation, Methodology, Validation, Writing – original draft, Writing – review & editing. **Mohammad Reza Hanafi:** Data curation, Investigation, Methodology, Validation, Visualization. **Augonis Algirdas:** Conceptualization, Investigation, Methodology, Supervision, Validation, Visualization. **Sahar Zinatloo-Ajabshir:** Conceptualization, Data curation, Investigation, Methodology, Supervision, Validation, Visualization.

Declaration of competing interest

The authors declare that they have no known competing financial interests or personal relationships that could have appeared to influence the work reported in this paper.

Data availability

No data was used for the research described in the article.

References

Adem, J.K., Seo, J., Park, S., Kim, G.M., 2025. Effects of low-lime calcium silicate cement addition on the hydration, carbonation, and microstructural characteristics of OPC pastes by carbonation curing. J. Build. Eng. 107, 112683. https://doi.org/10.1016/j.jobe.2025.112683, 2025/08/01/.

Adeyanju, E., Okeke, C.A., 2019. Exposure effect to cement dust pollution: a mini review. SN Appl. Sci. 1 (12), 1572. https://doi.org/10.1007/s42452-019-1583-0, 2019/11/08.

Alaloul, W.S., Al Salaheen, M., Alzubi, K., Musarat, M.A., 2024. Utilizing calcined and raw fly oil shale ash in the carbonation process of OPC cement-paste and mortar. Case Stud. Constr. Mater. 20, e02945. https://doi.org/10.1016/j.cscm.2024.e02945, 2024/07/01/.

Araos Henríquez, P., Aponte, D., Ibáñez-Insa, J., Barra Bizinotto, M., 2021. Ladle furnace slag as a partial replacement of Portland cement. Constr. Build. Mater. 289, 123106. https://doi.org/10.1016/j.conbuildmat.2021.123106, 2021/06/28/.

Asheghi Mehmandari, T., et al., 2024b. Flexural properties of fiber-reinforced concrete using hybrid recycled steel fibers and manufactured steel fibers. J. Build. Eng. 98, 111069. https://doi.org/10.1016/j.jobe.2024.111069, 2024/12/01/.

Asheghi Mehmandari, T., Shokouhian, M., Imani, M., Fahimifar, A., 2024a. Experimental and numerical analysis of tunnel primary support using recycled, and hybrid fiber reinforced shotcrete. Structures 63, 106282. https://doi.org/10.1016/j.istruc.2024.106282, 2024/05/01/.

ASTM C39, 2023. Standard test method for compressive strength of cylindrical concrete specimens. https://doi.org/10.1520/C0039_C0039M-21.

ASTM C469-02, 2017. Standard test method for static modulus of elasticity and poisson's ratio of concrete in compression. https://doi.org/10.1520/C0469-02.

ASTM C109/C109M-20, 2020. Standard test method for compressive strength of hydraulic cement mortars (using 2-in. or [50-mm] cube specimens). https://www.astm.org/c0109_c0109m-20.html.

Backes, J.G., Traverso, M., 2024. Social life cycle assessment in the construction industry: systematic literature review and identification of relevant social indicators for carbon reinforced concrete. Environ. Dev. Sustain. 26 (3), 7199–7233. https://doi.org/10.1007/s10668-023-03005-6, 2024/03/01.

Badalyan, M.M., et al., 2024. Effect of silica fume concentration and water–cement ratio on the compressive strength of cement-based mortars. Buildings 14 (3), 1–22. https://doi.org/10.3390/buildings14030757.

Barbero, I., Rezgui, Y., Beach, T., Petri, I., 2024. Social life cycle assessment in the construction sector: current work and directions for future research. Int. J. Life Cycle Assess. 29 (10), 1827–1845. https://doi.org/10.1007/s11367-024-02341-7, 2024/10/01.

Bildirici, M.E., Ersin, Ö.Ö., 2024. Cement production and CO2 emission cycles in the USA: evidence from MS-ARDL and MS-VARDL causality methods with century-long data. Environ. Sci. Pollut. Res. Int. 31 (24), 35369–35395. https://doi.org/10.1007/s11356-024-33489-2, 2024/05/01.

E. Bontempi, G. P. Sorrentino, A. Zanoletti, I. Alessandri, L. E. Depero, and A. Caneschi, "Sustainable materials and their contribution to the sustainable development goals (SDGs): a critical review based on an Italian example," Molecules, vol. 26, no. 5, doi: https://doi.org/10.3390/molecules26051407.

Bualuang, T., Jitsangiam, P., Chusai, N., Porninta, K., Rattanasak, U., Kua, H.W., 2025. Corn waste-derived biochar as a sustainable fine aggregate in pervious concrete for climate-resilient urban pavement applications. Dev. Built Environ. 23, 100735. https://doi.org/10.1016/j.dibe.2025.100735, 2025/10/01/.

Bualuang, T., Jitsangiam, P., Chusai, N., Suwan, T., Rattanasak, U., Chindaprasirt, P., 2024. Utilization of dumped coal ash from power-plant landfills for carbon footprint reduction in sustainable pavement base construction. Constr. Build. Mater. 441, 137462. https://doi.org/10.1016/j.conbuildmat.2024.137462, 2024/08/30/.

Cai, X., Cao, Z., Sun, J., Wang, H., Wu, S., 2024. Influence of steel slag on properties of cement-based materials: a review. Buildings 14 (9), 1–12. https://doi.org/10.3390/buildings14092985.

Chen, Y., et al., 2024. High-performance self-bonding bio-composites from wood fibers. Ind. Crops Prod. 209, 117944. https://doi.org/10.1016/j.indcrop.2023.117944, 2024/03/01/.

Czarnecka-Komorowska, D., Wachowiak, D., Gizelski, K., Kanciak, W., Ondrušová, D., Pajtášová, M., 2024. Sustainable composites containing post-production wood waste as a key element of the circular economy: processing and physicochemical properties. Sustainability 16 (4). https://doi.org/10.3390/su16041370.

Dahanni, H., Ventura, A., Le Guen, L., Dauvergne, M., Orcesi, A., Cremona, C., 2024. Life cycle assessment of cement: are existing data and models relevant to assess the cement industry's climate change mitigation strategies? A literature review. Constr. Build. Mater. 411, 134415. https://doi.org/10.1016/j.conbuildmat.2023.134415, 2024/01/12/.

Di Maria, A., Salman, M., Dubois, M., Van Acker, K., 2018. Life cycle assessment to evaluate the environmental performance of new construction material from stainless steel slag. Int. J. Life Cycle Assess. 23 (11), 2091–2109. https://doi.org/10.1007/s11367-018-1440-1, 2018/11/01.

Dias, S., et al., 2022. Lightweight cement composites containing end-of-life treated wood – leaching, hydration and mechanical tests. Constr. Build. Mater. 317, 125931. https://doi.org/10.1016/j.conbuildmat.2021.125931, 2022/01/24/.

Dong, Q., Wang, G., Chen, X., Tan, J., Gu, X., 2021. Recycling of steel slag aggregate in portland cement concrete: an overview. J. Clean. Prod. 282, 124447. https://doi.org/10.1016/j.jclepro.2020.124447, 2021/02/01/.

Ekinci, A., Hanafi, M., Ferreira, P.M.V., 2020. Influence of initial void ratio on critical state behaviour of poorly graded fine sands. Indian Geotech. J. 50 (5), 689–699. https://doi.org/10.1007/s40098-020-00416-4, 2020/10/01.

EN 15804+A2, 2019. Global Standard for Producing Environmental Product Declarations (EPD) for Construction Products.

Fahmi, A., Babaeian Amini, A., mohammadian, M., Rahimpour, H., 2023a. Sustainable and eco-friendly use of clay brick waste as an alumina-silicate base and different fillers for geopolymer brick production. J. Civ. Environ. Eng. 53 (112), 192–205. https://doi.org/10.22034/jcee.2022.50750.2126 (in en).

Fahmi, A., Zavaragh, S.R., Hanafi, M.R., Rahimpour, H., Zinatloo-Ajabshir, S., Asghari, A., 2023b. Facile preparation, characterization, and investigation of mechanical strength of starchy NaCl-binder as a lightweight construction material. Sci. Rep. 13 (1), 19042. https://doi.org/10.1038/s41598-023-46536-8, 2023/11/03.

Fei, H., et al., 2024. Photocatalytic performance and its internal relationship with hydration and carbonation of photocatalytic concrete: a review. J. Build. Eng. 97, 110782. https://doi.org/10.1016/j.jobe.2024.110782, 2024/11/15/.

Ghiasi, V., Marabi, Y., Fahmi, A., Maleki, H.R., Rahimpour, H., 2025. Compressive strength of geopolymer brick samples based on sand-washing waste with different particle sizes. Adv. Mater. Res. 14 (1), 31–42. https://doi.org/10.12989/amr.2025.14.1.031.

Gigar, F.Z., Khennane, A., Liow, J.-l., Tekle, B.H., Katoozi, E., 2023. Recycling timber waste into geopolymer cement bonded wood composites. Constr. Build. Mater. 400, 132793. https://doi.org/10.1016/j.conbuildmat.2023.132793, 2023/10/12.

Guleria, H., Goyal, S., 2025. Investigating the effect of accelerated carbonation curing duration on Portland and pozzolana cement-based concrete. Struct. Concr. n/a. https://doi.org/10.1002/suco.70326 n/a, 2025/10/01.

Hanafi, M.R., et al., 2025. Geopolymer from sand washing waste: mechanical, rheological, and sustainability perspectives. Results Eng. 28, 108060. https://doi.org/10.1016/j.rineng.2025.108060, 2025/12/01/.

Hanafi, M.R., Rahimpour, H., Zinatloo-Ajabshir, S., Moodi, F., Fahmi, A., 2024. Performance enhancement, life cycle assessment, and feature analysis of wheat starch-based NaCl-binder as a sustainable alternative to OPC mortar. Results Eng. 24, 103281. https://doi.org/10.1016/j.rineng.2024.103281, 2024/12/01/.

Hansted, F.A.S., Mantegazini, D.Z., Ribeiro, T.M., Gonçalves, C.E.C., Balestieri, J.A.P., 2022. A mini-review on the use of waste in the production of sustainable Portland cement composites. Waste Manag. Res. 41 (4), 828–838. https://doi.org/10.1177/0734242X22113524, 2023/04/01.

He, Z., Han, X., Zhang, Y., Zhang, Z., Shi, J., Gencel, O., 2022. Development of a new magnesium oxychloride cement board by recycling of waste wood, rice husk ash and flue gas desulfurization gypsum. J. Build. Eng. 61, 105206. https://doi.org/10.1016/j.jobe.2022.105206, 2022/12/01/.

Huang, W., Wang, H., 2024. Comprehensive assessment of engineering and environmental attributes of geopolymer pervious concrete with natural and recycled aggregate. J. Clean. Prod. 468, 143138. https://doi.org/10.1016/j.jclepro.2024.143138, 2024/08/25/.

Ibrahim, M., Alimi, W., Assaggaf, R., Salami, B.A., Oladapo, E.A., 2023. An overview of factors influencing the properties of concrete incorporating construction and demolition wastes. Constr. Build. Mater. 367, 130307. https://doi.org/10.1016/j.conbuildmat.2023.130307, 2023/02/27/.

Ige, O.E., Von Kallon, D.V., Desai, D., 2024. Carbon emissions mitigation methods for cement industry using a systems dynamics model. Clean Technol. Environ. Policy 26 (3), 579–597. https://doi.org/10.1007/s10098-023-02683-0, 2024/03/01.

ISO 14040:2006, Environmental Management - Life Cycle Assessment – Principles and Framework.

Jafari, P., Rasekh, E., Asheghi Mehmandari, T., Mohammadifar, M., Fahimifar, A., Jahed Armaghani, D., 2025. Upper-bound solutions for active face failure in shallow rectangular tunnels in anisotropic and non-homogeneous undrained clays. Geotech. Geol. Eng. 43 (3), 129. https://doi.org/10.1007/s10706-025-03086-2, 2025/03/02.

Jinanukul, P., et al., 2024. Comparative evaluation of mechanical and physical properties of mycelium composite boards made from Lentinus sajor-caju with various ratios of corn husk and sawdust. J. Fungi 10 (9). https://doi.org/10.3390/jof10090634.
Kang, X., Tian, Z., Choi, C.E., Ye, H., 2025. Reaction mechanisms of one-part and two-part slag-based binders activated by sodium carbonate and lime. Cem. Concr. Compos. 159, 105992. https://doi.org/10.1016/j.cemconcomp.2025.105992, 2025/05/01/.
Khankhaje, E., Kim, T., Jang, H., Kim, C.-S., Kim, J., Rafieizonooz, M., 2023. Properties of pervious concrete incorporating fly ash as partial replacement of cement: a review. Dev. Built Environ. 14, 100130. https://doi.org/10.1016/j.dibe.2023.100130, 2023/04/01/.
Krejsová, J., et al., 2024. Valorization of waste wood fly ash in environmentally friendly lime-based plasters with enhanced strengths for renovation purposes. J. Build. Eng. 87, 109056. https://doi.org/10.1016/j.jobe.2024.109056, 2024/06/15/.
Le, D.L., Salomone, R., Nguyen, Q.T., 2023. Circular bio-based building materials: a literature review of case studies and sustainability assessment methods. Build. Environ. 244, 110774. https://doi.org/10.1016/j.buildenv.2023.110774.
Li, J., Ji, Y.-X., Ni, X.-X., Lv, K.-H., Huang, X.-B., Sun, J.-S., 2024. A micro-crosslinked amphoteric hydrophobic association copolymer as high temperature- and salt-resistance fluid loss reducer for water-based drilling fluids. Pet. Sci. 21 (3), 1980–1991. https://doi.org/10.1016/j.petsci.2024.01.021, 2024/06/01/.
Li, L., Wu, M., 2022. An overview of utilizing CO2 for accelerated carbonation treatment in the concrete industry. J. CO2 Util. 60, 102000. https://doi.org/10.1016/j.jcou.2022.102000, 2022/06/01/.
Liang, X., Dong, H., Li, Z., Liu, C., Zhang, S., Ye, G., 2025. Characterization, pretreatment, and valorization of wood biomass fly ash in a binary cement-free binder. Dev. Built Environ. 23, 100700. https://doi.org/10.1016/j.dibe.2025.100700, 2025/10/01/.
Lin, R.-S., Liao, Y., Fu, C., Pan, T.-H., Guo, R., Wang, X.-Y., 2025. Mechanism analysis of microwave-carbonation solidification for carbide slag-based low-carbon materials. Cement Concr. Compos. 157, 105938. https://doi.org/10.1016/j.cemconcomp.2025.105938, 2025/03/01/.
Liu, J., Liu, Y., Zeng, J., Zhuge, Y., 2025a. A comprehensive review of mechanisms, techniques, and precursors in enforced carbonation for low-carbon concrete. J. Build. Eng. 112, 113685. https://doi.org/10.1016/j.jobe.2025.113685, 2025/10/15/.
Liu, Y., et al., 2025b. Impact resistance and enhancing mechanism of a novel mortar integrated with shear thickening fluid. Constr. Build. Mater. 498, 144036. https://doi.org/10.1016/j.conbuildmat.2025.144036, 2025/11/07/.
Liu, Z., et al., 2022. Study on wood chips modification and its application in wood-cement composites. Case Stud. Constr. Mater. 17, e01350. https://doi.org/10.1016/j.cscm.2022.e01350, 2022/12/01/.
Lu, S., et al., 2025. Research and application analysis on the pollution control of tail gas emissions from CO2 capture absorber. Results Eng. 25, 103677. https://doi.org/10.1016/j.rineng.2024.103677, 2025/03/01/.
Mehmandari, T.A., Shokouhian, M., Imani, M., Tee, K.F., Fahimifar, A., 2025. Split tensile behavior of recycled steel fiber-reinforced concrete. ACI Mater. J. 122 (2). https://doi.org/10.14359/51744375.
Miller, S.A., Moore, F.C., 2020. Climate and health damages from global concrete production. Nat. Clim. Change 10 (5), 439–443. https://doi.org/10.1038/s41558-020-0733-0, 2020/05/01.
Mohammadifar, M., Mehmandari, T.A., Mirjafari, S.A., 2024. Discovering the optimal distance between spatial orthogonal tunnels: a dynamic analysis using Tehran metro as a case study. Insight - Civ. Eng. 7 (1). https://doi.org/10.18282/ice.v7i1.613, 613–613.
Mollaei, S., Fahmi, A., Jahani, D., Babaei Golsefidi, Z., Babaei, R., Hanafi, M.R., 2023. A predictive model for the strength of a novel geopolymer construction material produced by autoclaved aerated concrete waste. Int. J. Sustain. Constr. Eng. Technol. 14 (1), 148–167. https://doi.org/10.30880/ijscet.2023.14.01.015. %02/%14.
Moodi, F., Hanafi, M.R., Shariatinia, Z., 2025. Toward high sustainability using fully recycled geopolymer concrete: mechanical, rheological, and microstructural properties. RSC Adv. 15 (28), 22953–22971. https://doi.org/10.1039/D5RA02249E.
Naseri, A., Maleki, B., Asheghi Mehmandari, T., Tohidi, A., Fahimifar, A., 2025. Investigating the influence of sample geometric variations on mechanical characterization in rock and concrete. J. Min. Environ. 16 (3), 1089–1107. https://doi.org/10.22044/jme.2024.14631.2759 (in en).
Nguyen, Q.H., Hanafi, M., Merkl, J.-P., d'Espinose de Lacaillerie, J.-B., 2021. Evolution of the microstructure of unconsolidated geopolymers by thermoporometry. J. Am. Ceram. Soc. 104 (3), 1581–1591. https://doi.org/10.1111/jace.17543, 2021/03/01.
Ozcelikci, E., Ozdogru, E., Tugluca, M.S., Ilcan, H., Sahmaran, M., 2024. Comprehensive investigation of performance of construction and demolition waste based wood fiber reinforced geopolymer composites. J. Build. Eng. 84, 108682. https://doi.org/10.1016/j.jobe.2024.108682, 2024/05/01/.
Peters, G.P., Marland, G., Le Quéré, C., Boden, T., Canadell, J.G., Raupach, M.R., 2012. Rapid growth in CO2 emissions after the 2008–2009 global financial crisis. Nat. Clim. Change 2 (1), 2–4. https://doi.org/10.1038/nclimate1332, 2012/01/01.
Pu, Q., et al., 2021. Systematic study of dynamic CO2 adsorption on activated carbons derived from different biomass. J. Alloys Compd. 887, 161406. https://doi.org/10.1016/j.jallcom.2021.161406, 2021/12/20/.
Qian, X., Xu, W., Wang, Y., Fang, H., Jing, Z., Chen, P., 2023. Revisiting the carbonation of recycled concrete fine: a pH-cycle carbonation method. J. Build. Eng. 77, 107438. https://doi.org/10.1016/j.jobe.2023.107438, 2023/10/15/.
Rahimpour, H., Amini, A.B., Sharifi, F., Fahmi, A., Zinatloo-Ajabshir, S., 2024. Facile fabrication of next-generation sustainable brick and mortar through geopolymerization of construction debris. Sci. Rep. 14 (1), 10914. https://doi.org/10.1038/s41598-024-61688-x, 2024/05/13.
Rahimpour, H., Esmaeili, J., 2025. Characterization, mechanical strength, rheological properties and life cycle assessment of fully recycled concrete through geopolymer technology. Sci. Rep. 15 (1), 9424. https://doi.org/10.1038/s41598-025-92307-y, 2025/03/19.
Rahmani, H., Algirdas, A., Shestavetska, A., Vaiciukyniene, D., 2025. Preparation and mechanical characterization of pressed carbonized wood sawdust bio-composite. Sci. Rep. 15 (1), 14981. https://doi.org/10.1038/s41598-025-98658-w, 2025/04/29.
Ren, P., Wang, A., Mo, K.H., Ling, T.-C., 2024. Fast-hardening production of high-strength BOFS aggregates by high-temperature carbonation curing. ACS Sustain. Chem. Eng. 12 (36), 13587–13597. https://doi.org/10.1021/acssuschemeng.4c04437, 2024/09/09.
Schmidt, W., et al., 2021. Sustainable circular value chains: from rural waste to feasible urban construction materials solutions. Dev. Built Environ. 6, 100047. https://doi.org/10.1016/j.dibe.2021.100047, 2021/05/01/.
Sharma, R.D., Singh, N., 2023. Evaluation of strength and absorption behaviour of iron slag and recycled aggregates concrete and its comparative environmental estimation by life cycle assessment. Clean. Mater. 10, 100210. https://doi.org/10.1016/j.clema.2023.100210, 2023/12/01/.
Steger, L., Blotevogel, S., Frouin, L., Patapy, C., Cyr, M., 2021. Experimental evidence for the acceleration of slag hydration in blended cements by the addition of CaCl2. Cement Concr. Res. 149, 106558. https://doi.org/10.1016/j.cemconres.2021.106558, 2021/11/01/.
Torres-Ortega, R., Torres-Sanchez, D., Lopez-Lara, T., 2025. Mechanical properties of hydraulic concretes with partial replacement of Portland cement by pozzolans obtained from agro-industrial residues: a review. Heliyon 11 (1), e41004. https://doi.org/10.1016/j.heliyon.2024.e41004.
Tsakiridis, P.E., Papadimitriou, G.D., Tsivilis, S., Koroneos, C., 2008. Utilization of steel slag for Portland cement clinker production. J. Hazard. Mater. 152 (2), 805–811. https://doi.org/10.1016/j.jhazmat.2007.07.093, 2008/04/01/.
Wang, J., Pu, Q., Ning, P., Lu, S., 2021. Activated carbon-based composites for capturing CO2: a review. Greenhouse Gases: Sci. Technol. 11 (2), 377–393. https://doi.org/10.1002/ghg.2051, 2021/04/01.
Wu, M., Liu, Z., Wang, H., Zhou, H., Wang, X., 2025b. Cyclic fatigue effect on mechanical property change of hot dry rock in wellbores of enhanced geothermal systems. Int. J. Rock Mech. Min. Sci. 195, 106303. https://doi.org/10.1016/j.ijrmms.2025.106303, 2025/11/01/.
Wu, Z., Pei, T., Bao, Z., Ng, S.T., Lu, G., Chen, K., 2025a. Utilizing intelligent technologies in construction and demolition waste management: from a systematic review to an implementation framework. Front. Eng. Manag. 12 (1), 1–23. https://doi.org/10.1007/s42524-024-0144-4, 2025/03/01.
Yang, Q., Liu, Z., Wang, X., Liu, B., Tian, F., Wang, X., 2025. Physical model test and numerical modeling of cross-sectional shape effect on evolution mechanism of time-delayed deformation and rockburst in deep tunnels. Rock Mech. Rock Eng. https://doi.org/10.1007/s00603-025-04906-w, 2025/09/09.
Yang, X.P., Jiang, Y.Z., Lu, S.J., Jiang, D.W., 2013. The developing of high efficiency coal-fired flue gas CO2 capturing absorbent. Adv. Mater. Res. 641, 136–139. https://doi.org/10.4028/www.scientific.net/AMR.641-642.136.
Yilmazoglu, A., Yildirim Salih, T., Yıldız, S., Behçet Ömer, F., 2024. Effect of GGBS content and water/geopolymer solid ratio on the mechanical, elevated temperature resistance, and sorptivity properties of FA/GGBS-Based geopolymer concrete. J. Mater. Civ. Eng. 36 (4), 04024032. https://doi.org/10.1061/JMCEE7.MTENG-17167, 2024/04/01.
Zhang, K., Wang, C., Zhao, Y., Bi, J., Shen, M., Deng, X., 2024. Study on the effect of wood admixture on the physical and mechanical properties of corn cob ecological recycled concrete. J. Build. Eng. 88, 109116. https://doi.org/10.1016/j.jobe.2024.109116, 2024/07/01/.
Zhang, Y., et al., 2025. A review on curve edge based architectures under lateral loads. Thin-Walled Struct. 217, 113849. https://doi.org/10.1016/j.tws.2025.113849, 2025/12/01/.
Zhou, H., Liu, Z., Shao, J., Shen, W., Hamdi, E., 2025. Effects of stress direction and magnitude on strength and failure of weakly anisotropic sandstone under true triaxial compression. Rock Mech. Rock Eng. https://doi.org/10.1007/s00603-025-04982-y, 2025/10/14.